Morphogen transport in epithelia

T. Bollenbach,[1,*] K. Kruse,[1,†] P. Pantazis,[2,‡] M. González-Gaitán,[2,§] and F. Jülicher[1,‖]
[1]*Max-Planck-Institute for the Physics of Complex Systems, Nöthnitzer Strasse 38, 01187 Dresden, Germany*
[2]*Max-Planck-Institute of Molecular Cell Biology and Genetics, Pfotenhauer Strasse 108, 01307 Dresden, Germany*
(Received 11 August 2006; published 2 January 2007)

We present a general theoretical framework to discuss mechanisms of morphogen transport and gradient formation in a cell layer. Trafficking events on the cellular scale lead to transport on larger scales. We discuss in particular the case of transcytosis where morphogens undergo repeated rounds of internalization into cells and recycling. Based on a description on the cellular scale, we derive effective nonlinear transport equations in one and two dimensions which are valid on larger scales. We derive analytic expressions for the concentration dependence of the effective diffusion coefficient and the effective degradation rate. We discuss the effects of a directional bias on morphogen transport and those of the coupling of the morphogen and receptor kinetics. Furthermore, we discuss general properties of cellular transport processes such as the robustness of gradients and relate our results to recent experiments on the morphogen Decapentaplegic (Dpp) that acts in the wing disk of the fruit fly Drosophila.

DOI: 10.1103/PhysRevE.75.011901 PACS number(s): 87.16.Uv, 87.18.La, 87.17.Aa

I. INTRODUCTION

Morphogens are signaling molecules which are secreted from cells in a restricted source region and provide signals to cells located at a distance from this source. They play a key role for the determination of cell fates in animal development [1]. While the term "morphogen" was coined by Turing in his seminal work on pattern formation in reaction-diffusion systems [2], the modern paradigm of morphogen action was introduced by Wolpert in 1969 [3]. According to this paradigm, morphogens spread from the source region into the adjacent target tissue where they are partly degraded. The combination of the localized production of morphogens, transport, and degradation leads to the formation of a nonequilibrium steady state in which the morphogen concentration decreases with increasing distance from the morphogen source. This concentration profile is called "morphogen gradient" and contains positional information about the distance from the morphogen source. Cells in the tissue detect the local morphogen concentration via receptor molecules that are present on their surface and respond by expressing a set of target genes in a manner that depends on the detected morphogen concentration. In this way, the morphogen gradient can generate a pattern of differentiated cells in the target tissue. In the last two decades, the existence of morphogen gradients has been supported by considerable experimental evidence. Prominent examples of signaling molecules that function as morphogens are Bicoid which acts in the embryo of the fruit fly Drosophila [4,5], Decapentaplegic (Dpp) which acts in the Drosophila wing disk [6,7], and Activin which acts in the embryo of the frog Xenopus [8].

The mechanisms by which morphogens are transported and gradients are formed are so far not well understood. A difficulty in the study of morphogen kinetics is the fact that morphogen transport in a tissue is coupled to cellular trafficking processes. It is influenced, for example, by ligand-receptor binding, the endocytosis of ligand-receptor pairs, and the kinetics of receptor numbers. For a long time, it was taken for granted that morphogens move by diffusion in the extracellular space surrounding the cells [9]. In a few cases, there is experimental evidence for this: the morphogen Activin in Xenopus is an example [10]. However, for one of the best studied model systems, the morphogen Dpp in the Drosophila wing disk, experiments have called diffusive transport into question and suggested an important role of cell surface molecules in this process [6,11]. Consequently, other transport mechanisms than extracellular diffusion have been suggested [6,11,12]. First, Dpp could be transported by transcytosis. Here, transport is achieved via repeated rounds of morphogen binding to cell surface receptors, internalization into the cell and subsequent externalization, and release of the ligand from the receptor at a different position on the cell surface [6,13]. Second, Dpp might move by passive diffusion on the cell surface. Here, a certain type of large molecules (called Heparan Sulfate Proteoglycans, HSPGs) which are located on the cell surface could function as a "carrier" for the morphogens [11]. Furthermore, morphogen transport could occur in cytonemes which are long membrane tubes that connect the morphogen source cells to cells in the target tissue [12]. Due to the complexity of the problem, a combination of theoretical descriptions of morphogen gradient formation and systematic experiments is needed to identify the dominant morphogen transport mechanism [13,14].

During animal development, the precision of the positions of differentiating cells in the tissue and the times at which cells differentiate is typically high [15,16]. This indicates that robust mechanisms that are insensitive to changes of

*Present address: Department of Systems Biology, Harvard Medical School, 200 Longwood Avenue, Boston, MA 02115, USA.
†Present address: Theoretische Physik, Universität des Saarlandes, Postfach 151150, 66041 Saarbrücken, Germany.
‡Present address: California Institute of Technology, 1200 E. California Blvd., MC 139-74, Pasadena, CA 91125, USA.
§Corresponding author. Present address: Department of Biochemistry, Sciences II, 30 Quai Ernest-Ansermet, 1211 Geneva 4, Switzerland. Electronic address: Marcos.Gonzalez@biochem.unige.ch
‖Corresponding author. Electronic address: julicher@pks.mpg.de

environmental conditions and to intrinsic fluctuations have evolved to control cell differentiation. Clearly, such robustness could be achieved if morphogen gradients are themselves robust. Evidence for the robustness of morphogen gradients was found in recent experiments [17–19]. This robustness must originate in the mechanisms by which morphogens are transported and degraded. The robustness and precision of morphogen gradients [16,18–21] or a possible role of anomalous diffusion in morphogen transport [22] can only be understood using a combination of theoretical and experimental efforts.

In this article, we provide a detailed description of morphogen gradient formation by different mechanisms and provide full derivations of the morphogen transport equations. Our description captures several processes that are supported by experimental data for the morphogen Dpp in the Drosophila wing disk. These experimental findings will be briefly summarized in Sec. II. While we focus on the wing disk of the fruit fly here, these processes are very likely to play an important role for morphogen gradient formation in other animals. Starting from a description of cellular trafficking processes, we derive in Sec. III effective transport equations on larger scales. We investigate key properties of gradient formation by these mechanisms in Sec. IV and study the effects of a directional bias for transport resulting from cellular polarity. Finally, we extend our approach to higher dimensions in Sec. V and discuss morphogen transport in two-dimensional epithelia.

This article extends and complements our recent work on morphogen gradient formation [20]. In our previous work, we highlighted key results of our analysis, in particular the robustness of steady state gradients formed by transcytosis [20]. Here, we discuss the underlying theoretical framework in detail and extend it to higher dimensions and to various other transport scenarios. For the sake of completeness, we briefly recall some of the results of [20].

II. MORPHOGEN GRADIENT FORMATION AND CELLULAR TRAFFICKING PROCESSES

The larva of the fruit fly Drosophila contains precursors of the organs of the adult animal. The precursor of the fly wing is a flat pouch that consists of two cell layers that are connected at the edges and is called wing disk (see Fig. 1 in [13]). The thicker one of these cell layers is formed by columnar epithelial cells and includes the so-called wing primordium. In the following, we consider this two-dimensional cell layer [13,14]. Dpp is produced and secreted in a specific source region which is a narrow stripe with a width of about 7 cell diameters that is located at the center of this layer. Cells outside of this source do not produce Dpp but possess receptors located at their cell surface to detect its presence. Dpp spreads from the source region into the adjacent target tissue on both sides of the source region. In the whole tissue, Dpp molecules are degraded. As a consequence of the localized source and degradation, a graded morphogen profile is built up. This formation of the morphogen gradient can be directly observed in experiments by using a Dpp that is labeled with green fluorescent protein (GFP-Dpp) [6,7]. In steady state, the Dpp gradient extends over 50 μm into the target tissue. This corresponds to about 20 cell diameters.

Several cellular processes are relevant during the formation of this morphogen gradient. Morphogens are ligands which bind to specific receptor molecules. Ligand-receptor pairs are internalized into the cell via endocytosis. Internalized ligands are either degraded or they can be recycled to the cell surface via exocytosis. Finally, receptor-ligand pairs can diffuse on the cell surface [23] and free ligands can diffuse in the extracellular space surrounding the cells.

Furthermore, cells in the wing disk produce, degrade, externalize, and internalize receptor molecules. In general, the production rate of these receptors is affected by the local morphogen concentration. For example, a high Dpp concentration leads to a reduced production rate of the Dpp receptor Thick-veins (Tkv) in the wing disk [7]. This behavior is called "receptor down-regulation." The opposite behavior can also occur: high concentrations of Hedgehog, another morphogen acting in the wing disk, lead to an increased production of its receptor Patched [24]. This phenomenon is called "receptor up-regulation."

Recent experiments have revealed the interplay of Dpp gradient formation and cellular trafficking. First, endocytosis has been blocked in the whole wing disk except for the Dpp source region or, alternatively, in smaller patches of cells (clones) in the tissue [6,13]. This has been achieved using mutant flies in which endocytosis can be blocked at an elevated temperature of 34 °C due to the temperature-sensitive mutation shibire. Five hours upon blocking endocytosis in the whole target tissue, GFP-Dpp fluorescence was almost undetectable in the target tissue while its gradient extended visibly over more than 20 cell diameters into this tissue before the endocytic block. When endocytosis was only blocked in patches of cells near the Dpp source region, a pronounced transient depletion of the GFP-Dpp concentration behind these clones was observed. Both experiments indicate a role of endocytosis in Dpp transport. This suggests that instead of simply diffusing in the extracellular space, Dpp is transported via the cell interior in repeated rounds of endocytosis and exocytosis. This transport mechanism is called transcytosis [6]. Indeed, a theoretical description in which morphogen transport is solely based on extracellular diffusion while interactions of the morphogen with its receptors are taken into account was found to be inconsistent with the experimental observations [13].

In a different set of experiments, the role of large cell surface molecules (HSPGs) in morphogen transport was investigated [11]. A depletion of extracellular Dpp was observed behind mutant clones of cells which lack HSPGs. This indicates a role of HSPGs in Dpp transport. Indeed, it has been suggested that HSPGs facilitate the diffusion of morphogens on the cell surface [11].

III. MORPHOGEN TRANSPORT IN ONE DIMENSION

We introduce a discrete description of morphogen transport by transcytosis and passive extracellular diffusion and derive transport equations for these processes. The theoretical description developed here is generally applicable to bio-

logical systems in which molecules are transported by extracellular diffusion and transcytosis. To stress this generality, we will mostly refer to the transported molecules as "ligands" instead of "morphogens."

A. Ligand kinetics in a chain of cells

In one space dimension, we describe the ligand kinetics in a chain of cells, see Fig. 1. We denote the distance between the centers of two neighboring cells by a and the width of the gap between two cells by b. In this chain, n indexes the cells, see Fig. 1. The number of free extracellular ligands between cells n and $n+1$ is denoted L_n. The numbers of intracellular free and ligand-bound receptors are denoted $R_n^{(\mathrm{i})}$ and $S_n^{(\mathrm{i})}$, respectively. $R_n^{(\mathrm{l})}$ and $R_n^{(\mathrm{r})}$ denote the concentrations of free receptors on the left and right cell surfaces, respectively. $S_n^{(\mathrm{l})}$ and $S_n^{(\mathrm{r})}$ denote the ligand-bound receptors accordingly. The kinetics of the ligand and receptor numbers are given by

$$\frac{d}{dt}L_n = k_{\mathrm{off}}(S_n^{(\mathrm{r})} + S_{n+1}^{(\mathrm{l})}) - k_{\mathrm{on}}(R_n^{(r)} + R_{n+1}^{(\mathrm{l})})L_n + \frac{D_0}{a^2}(L_{n+1} + L_{n-1} - 2L_n) - e_{\mathrm{deg}}L_n,$$

$$\frac{d}{dt}R_n^{(\mathrm{r})} = \frac{f_{\mathrm{syn}}}{2} + k_{\mathrm{off}}S_n^{(\mathrm{r})} - k_{\mathrm{on}}R_n^{(\mathrm{r})}L_n - f_{\mathrm{int}}R_n^{(\mathrm{r})} + \frac{f_{\mathrm{ext}}}{2}R_n^{(\mathrm{i})},$$

$$\frac{d}{dt}S_n^{(\mathrm{r})} = -k_{\mathrm{off}}S_n^{(\mathrm{r})} + k_{\mathrm{on}}R_n^{(\mathrm{r})}L_n - b_{\mathrm{int}}S_n^{(\mathrm{r})} + \frac{b_{\mathrm{ext}}}{2}S_n^{(\mathrm{i})},$$

$$\frac{d}{dt}R_n^{(\mathrm{l})} = \frac{f_{\mathrm{syn}}}{2} + k_{\mathrm{off}}S_n^{(\mathrm{l})} - k_{\mathrm{on}}R_n^{(\mathrm{l})}L_{n-1} - f_{\mathrm{int}}R_n^{(\mathrm{l})} + \frac{f_{\mathrm{ext}}}{2}R_n^{(\mathrm{i})},$$

$$\frac{d}{dt}S_n^{(\mathrm{l})} = -k_{\mathrm{off}}S_n^{(\mathrm{l})} + k_{\mathrm{on}}R_n^{(\mathrm{l})}L_{n-1} - b_{\mathrm{int}}S_n^{(\mathrm{l})} + \frac{b_{\mathrm{ext}}}{2}S_n^{(\mathrm{i})},$$

$$\frac{d}{dt}R_n^{(\mathrm{i})} = -f_{\mathrm{ext}}R_n^{(\mathrm{i})} + f_{\mathrm{int}}(R_n^{(\mathrm{l})} + R_n^{(\mathrm{r})}) - f_{\mathrm{deg}}R_n^{(\mathrm{i})},$$

$$\frac{d}{dt}S_n^{(\mathrm{i})} = -b_{\mathrm{ext}}S_n^{(\mathrm{i})} + b_{\mathrm{int}}(S_n^{(\mathrm{l})} + S_n^{(\mathrm{r})}) - b_{\mathrm{deg}}S_n^{(\mathrm{i})}. \quad (1)$$

Here, the binding and un-binding of ligands to and from receptors is characterized by rates k_{on} and k_{off}. The internalization and externalization of receptor-ligand complexes is captured by the rates b_{int} and b_{ext}. Free ligands can hop directly from one gap between the cells to the adjacent ones at a rate $2D_0/a^2$. This describes their free diffusion in the extracellular space around the cells with diffusion coefficient D_0. The degradation of ligands in the extracellular space occurs with rate e_{deg} and that of ligands bound to receptors inside the cell with rate b_{deg}. Furthermore, free receptors are internalized and externalized with rates f_{int} and f_{ext}, respectively. Internalized free receptors are degraded with rate f_{deg}. In addition, each cell produces receptors with a rate f_{syn}.

Newly produced receptors appear on the cell surface [25]. The rate of receptor synthesis f_{syn} in Eq. (1) depends on $R_n^{(\mathrm{l})}+R_n^{(\mathrm{r})}$ and $S_n^{(\mathrm{l})}+S_n^{(\mathrm{r})}$:

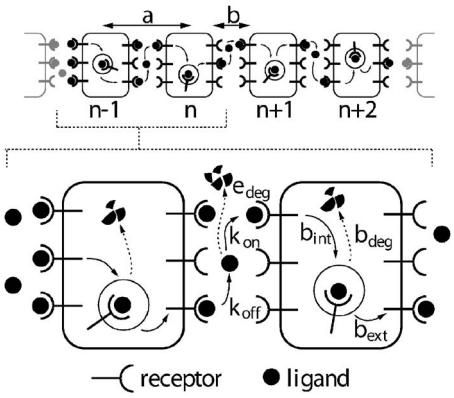

FIG. 1. Schematic representation of ligand transport by transcytosis in a chain of cells of diameter a indexed by n. The rates of ligand-receptor binding and un-binding, internalization and externalization of ligand-receptor pairs are denoted k_{on}, k_{off}, b_{int}, and b_{ext}. Degradation of ligand occurs inside the cells with rate b_{deg} and in the extracellular space with rate e_{deg}. Ligands can also hop directly between neighboring extracellular spaces at a rate $2D_0/a^2$ which describes their movement in the extracellular space around the cells by passive diffusion with diffusion coefficient D_0 (not shown). Figure modified from [20] .

$$f_{\mathrm{syn}} = f_{\mathrm{syn}}^0\left(1 - \frac{R_n^{(\mathrm{l})} + R_n^{(\mathrm{r})} + \psi(S_n^{(\mathrm{l})} + S_n^{(\mathrm{r})})}{R_{\mathrm{max}}}\right), \quad (2)$$

where f_{syn}^0 is a basal rate of receptor synthesis and R_{max} is the saturation value of the surface receptor concentration at which the production of new receptors stops. The dimensionless parameter ψ couples receptor synthesis to the concentration of morphogens. The two cases of receptor up- and down-regulation [25] are captured by $\psi<1$ and $\psi>1$, respectively.

The description (1) is valid in the bulk of the system. We still have to specify the kinetics at the boundaries of the chain. To describe the effects of a ligand source located at $n=0$ in Eq. (1), we modify the equation for the free ligand:

$$\frac{d}{dt}L_0 = k_{\mathrm{off}}S_1^{(\mathrm{l})} - k_{\mathrm{on}}R_1^{(\mathrm{l})}L_0 + \frac{D_0}{a^2}(L_1 - L_0) - e_{\mathrm{deg}}L_0 + \nu, \quad (3)$$

where ν is the rate at which ligands from the source enter the system. At the position $n=N$ where the lattice ends, we impose

$$\frac{d}{dt}L_N = k_{\mathrm{off}}S_N^{(\mathrm{r})} - k_{\mathrm{on}}R_N^{(\mathrm{r})}L_N + \frac{D_0}{a^2}(L_{N-1} - L_N) - e_{\mathrm{deg}}L_N, \quad (4)$$

which describes a zero flux boundary condition at this edge of the lattice. This boundary condition can be motivated by the geometry of the Drosophila wing disk [13]. However, if N is sufficiently large the ligand number at N is small and the choice of boundary condition has only a small influence on the ligand profile. A sequence of morphogen and receptor profiles at different times that were obtained by numerical solution of Eq. (1) are presented in Fig. 2 together with the steady state profiles that represent the morphogen gradient.

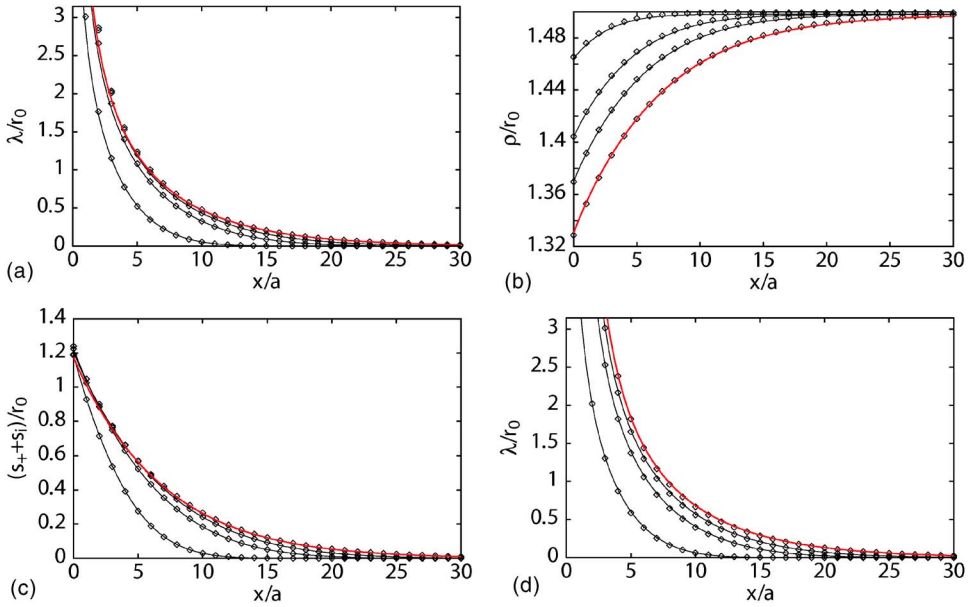

FIG. 2. (Color online) Time development of gradient formation in our description of ligand transport. Ligand densities in the presence of a source at $x=0$ at different times $tb_{\mathrm{deg}}=0.72, 2.16, 3.6$ during gradient formation (black lines) and in steady state (red lines). Lines indicate solutions to Eq. (6), while symbols indicate solutions to Eq. (1) for comparison. (a–c) Time development of the profiles of the total ligand density $\lambda(x,t)$ (a), the total receptor density $\rho(x,t)$ (b), and the receptor bound ligand density $s_i(x,t)+s_+(x,t)$ (c) in the absence of extracellular diffusion, i.e., for $D_0=0$. (d) Like (a) but with $2D_0/a^2b_{\mathrm{deg}}=10/3$, i.e., in the presence of extracellular diffusion. All concentrations are normalized to the steady state value of the surface receptor concentration in the absence of ligands r_0. Initial conditions at $t=0$: $\lambda(x)=0$ and $\rho(x)=(1+f_{\mathrm{int}}/f_{\mathrm{ext}})r_0$. Parameters are $k_{\mathrm{off}}/b_{\mathrm{deg}}=b_{\mathrm{int}}/b_{\mathrm{deg}}=f_{\mathrm{int}}/b_{\mathrm{deg}}=1000/3$, $k_{\mathrm{on}}ar_{\mathrm{max}}/b_{\mathrm{deg}}=8000/3$, $b_{\mathrm{ext}}/b_{\mathrm{deg}}=f_{\mathrm{ext}}/b_{\mathrm{deg}}=2000/3$, $e_{\mathrm{deg}}/b_{\mathrm{deg}}=2/3$, $f_{\mathrm{deg}}/b_{\mathrm{deg}}=1$, $f^0_{\mathrm{syn}}/ar_{\mathrm{max}}b_{\mathrm{deg}}=1/12$, $\psi=2$, $j_0/b_{\mathrm{deg}}ar_{\mathrm{max}}=25/6$, $r_0/r_{\mathrm{max}}=1/7$, and $j=0$ at $x/a=50$.

B. Effective transport equations on larger scales

We derive effective continuum transport equations for ligand transport starting from Eq. (1). We introduce the concentrations $l(t,x)=L_n(t)/a$, $r^{(\mathrm{l})}(t,x)=R^{(\mathrm{l})}_n(t)/a$, $r^{(\mathrm{r})}(t,x)=R^{(\mathrm{r})}_n(t)/a$, $r_i(t,x)=R^{(\mathrm{i})}_n(t)/a$, $s^{(\mathrm{l})}(t,x)=S^{(\mathrm{l})}_n(t)/a$, $s^{(\mathrm{r})}(t,x)=S^{(\mathrm{r})}_n(t)/a$, and $s_i(t,x)=S^{(\mathrm{i})}_n(t)/a$ where $x=na$. We derive continuum equations for the kinetics of these densities starting from Eq. (1) by locally expanding the densities in a power series with respect to x, for example, $L_{n+1}/a=l(x+a)=l(x)+a\partial_x l(x)+a^2\partial_x^2 l(x)/2$. It is further useful to introduce the new variables $r_\pm(t,x)=r^{(\mathrm{l})}(t,x)\pm r^{(r)}(t,x)$ and $s_\pm(t,x)=s^{(\mathrm{l})}(t,x)\pm s^{(\mathrm{r})}(t,x)$ so that r_+ and s_+ measure the total free and ligand bound surface receptor concentrations per cell and r_- and s_- the polarization of these concentrations on the cell surface, respectively.

In situations where the length ξ_D over which the steady state gradient decays is large compared to the cell diameter a, a separation of time scales occurs in the system which makes the adiabatic elimination of rapid variables possible. Indeed, if τ_a is the relaxation time of the kinetics within one cell, the slow relaxation of the gradient occurs on a time scale $\tau_{\xi_D}=\tau_a(\xi_D/a)^2 \gg \tau_a$. We thus use the approximation that all local kinetics relaxes instantaneously. At each position x, this yields the relations

$$l=\frac{k_{\mathrm{off}}s_+}{k_{\mathrm{on}}ar_+},$$

$$s_i=\frac{b_{\mathrm{int}}s_+}{b_{\mathrm{ext}}},$$

$$s_-=\frac{k_{\mathrm{on}}alr_- - \frac{abk_{\mathrm{on}}}{2}r_+\partial_x l+\frac{(a-b)b_{\mathrm{ext}}}{2}\partial_x s_i}{b_{\mathrm{int}}+k_{\mathrm{off}}},$$

$$r_i=\frac{f_{\mathrm{int}}r_+}{f_{\mathrm{ext}}},$$

$$r_-=\frac{k_{\mathrm{off}}s_- + \frac{abk_{\mathrm{on}}}{2}r_+\partial_x l+\frac{(a-b)f_{\mathrm{ext}}}{2}\partial_x r_i}{f_{\mathrm{int}}+k_{\mathrm{on}}al}. \tag{5}$$

Using these expressions, we can adiabatically eliminate five of the seven variables $l,s_i,s_+,s_-,r_i,r_+,r_-$ and obtain only two coupled equations for the remaining slow variables which are the total ligand density $\lambda(x,t)=l(x,t)+s_i(x,t)+s_+(x,t)$ and the total receptor density $\rho(x,t)=r_i(x,t)+r_+(x,t)+s_i(x,t)+s_+(x,t)$:

$$\partial_t\lambda=\partial_x(D_\lambda(\lambda,\rho)\partial_x\lambda+D_\rho(\lambda,\rho)\partial_x\rho)-k_\lambda(\lambda,\rho)\lambda, \tag{6}$$

$$\partial_t\rho=\nu_{\mathrm{syn}}(\lambda,\rho)-k_\rho(\lambda,\rho)\rho. \tag{7}$$

The other densities $l,s_i,s_+,s_-,r_i,r_+,r_-$ can be calculated from λ, ρ, and their first spatial derivatives via Eq. (5). The derivation of Eqs. (5)–(7) is discussed in Appendix A. In addition to Eqs. (6) and (7), this procedure provides us with

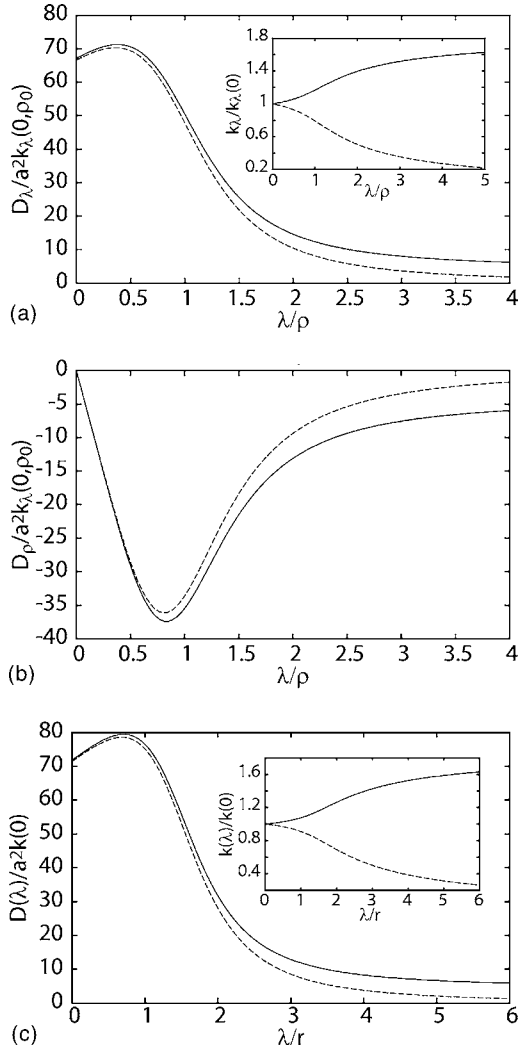

FIG. 3. Effective transport coefficients and degradation rates for transcytosis. (a,b) Coefficients $D_\lambda(\lambda,\rho)$, $D_\rho(\lambda,\rho)$, and $k_\lambda(\lambda,\rho)$ in the transport equation (6) as a function of the dimensionless ratio λ/ρ of the total ligand concentration λ and the total receptor concentration ρ. The solid lines show the coefficients D_λ and D_ρ in presence of extracellular diffusion with $2D_0/a^2b_{\rm deg}=10/3$. Broken lines show these coefficients in the absence of extracellular diffusion, i.e., with $D_0=0$. Inset in (a): the solid line shows k_λ with $e_{\rm deg}/b_{\rm deg}=2/3$ and the broken line with $e_{\rm deg}=0$. ρ_0 denotes the steady state total receptor concentration in the absence of ligands. (c) Effective diffusion coefficient $D(\lambda)$ in the transport equation for the constant surface receptor approximation (11) as a function of the ligand concentration λ/r for $2D_0/a^2b_{\rm deg}=10/3$ (solid line) and $D_0=0$ (dashed line). Inset: effective degradation rate $k(\lambda)$ as a function of λ/r for $e_{\rm deg}=0$ (dashed line) and $e_{\rm deg}/b_{\rm deg}=2/3$ (solid line). The constant total surface receptor concentration is denoted r. Parameters as in Fig. 2 with $k_{\rm on}a\rho/b_{\rm deg}=8000/3$ in (a) and (b) and $k_{\rm on}ar/b_{\rm deg}=8000/3$ in (c).

explicit expressions for the effective diffusion coefficient D_λ, the effective degradation rate k_λ, the receptor degradation rate k_ρ as well as the transport coefficient D_ρ which describes ligand transport induced by gradients of the receptor concentration, see Eq. (A6). In Figs. 3(a) and 3(b), the coefficients D_λ, D_ρ, and k_λ are displayed as a function of the ligand concentration λ for a typical choice of parameters. The effective receptor production rate $\nu_{\rm syn}(\lambda,\rho)=f_{\rm syn}/a$ is a function of the ligand and receptor concentrations. The functional form of $\nu_{\rm syn}$ that corresponds to the receptor production rate (2) in the discrete description is

$$\nu_{\rm syn}(\lambda,\rho)=\frac{f_{\rm syn}^0}{a}\left(1-\frac{r_+(\lambda,\rho)+\psi s_+(\lambda,\rho)}{r_{\rm max}}\right), \tag{8}$$

with $r_{\rm max}=R_{\rm max}/a$. Ligand transport is associated with the current $j=-[D_\lambda(\lambda,\rho)\partial_x\lambda+D_\rho(\lambda,\rho)\partial_x\rho]$. The current j_0 at $x=0$ is related to the secretion rate ν in Eq. (3). In one dimension $j_0=\nu$.

In Fig. 2 we show time-dependent receptor and ligand profiles which are solutions to Eqs. (6) and (7). These solutions are in agreement with the corresponding solutions to the discrete description (1) which validates the adiabatic approximation made in the derivation of Eqs. (6) and (7).

C. Effects of a directional bias

If cells possess a polarity, transcytosis can have a bias and lead to directed transport. Here, we include a directional bias in our description of ligand transport. Experiments indicate that the transport of the morphogen Dpp in the Drosophila wing disk is nondirectional on macroscopic length scales [6]. However, epithelia with cell polarity could in principle exhibit directional transcytosis.

We therefore generalize the discrete description (1) by allowing receptor-bound ligand molecules to be preferentially externalized on either the left or the right cell surface. To this end, we introduce a dimensionless parameter β which measures this bias: for $\beta=-1/2$, all receptor-bound ligands are externalized on the left surface, for $\beta=1/2$ on the right surface, and for $\beta=0$, we recover the unbiased description, see Appendix B for details.

In the presence of such a bias, the transport equations (6) and (7) generalize to

$$\partial_t\lambda=\partial_x(D_\lambda(\lambda,\rho)\partial_x\lambda+D_\rho(\lambda,\rho)\partial_x\rho-V_\beta(\lambda,\rho)\lambda)-k_\lambda(\lambda,\rho)\lambda,$$

$$\partial_t\rho=\nu_{\rm syn}(\lambda,\rho)-k_\rho(\lambda,\rho)\rho, \tag{9}$$

where $V_\beta(\lambda,\rho)$ is a concentration-dependent effective drift velocity, see Eq. (B3). The other coefficients in Eq. (9) remain the same as in the case without directional bias. In Fig. 4(a), we show V_β as a function of λ for $\beta=0.1$, i.e., a bias that leads to preferential transport to the right. Typical ligand and receptor profiles that are generated in the presence of a bias are shown in Figs. 4(b) and 4(c).

D. Constant surface receptor concentration

We now discuss the simple case where the total surface receptor number R is constant everywhere. This approximation is useful because it still captures most important features of morphogen transport by transcytosis [20].

In this case the receptor kinetics in Eq. (1) becomes obsolete. The equations describing ligand transport in this simple case are

$$\frac{d}{dt}L_n = k_{\text{off}}(S_n^{(\text{r})} + S_{n+1}^{(\text{l})}) - k_{\text{on}}(R - S_n^{(\text{r})} - S_{n+1}^{(\text{l})})L_n + \frac{D_0}{a^2}(L_{n+1} + L_{n-1} - 2L_n) - e_{\text{deg}}L_n,$$

$$\frac{d}{dt}S_n^{(\text{r})} = -k_{\text{off}}S_n^{(\text{r})} + k_{\text{on}}\left(\frac{R}{2} - S_n^{(\text{r})}\right)L_n - b_{\text{int}}S_n^{(\text{r})} + \frac{1}{2}b_{\text{ext}}S_n^{(\text{i})},$$

$$\frac{d}{dt}S_n^{(\text{l})} = -k_{\text{off}}S_n^{(\text{l})} + k_{\text{on}}\left(\frac{R}{2} - S_n^{(\text{l})}\right)L_{n-1} - b_{\text{int}}S_n^{(\text{l})} + \frac{1}{2}b_{\text{ext}}S_n^{(\text{i})},$$

$$\frac{d}{dt}S_n^{(\text{i})} = -b_{\text{ext}}S_n^{(\text{i})} + b_{\text{int}}(S_n^{(\text{l})} + S_n^{(\text{r})}) - b_{\text{deg}}S_n^{(\text{i})}. \quad (10)$$

Boundary conditions analogous to Eqs. (3) and (4) are imposed at $n=0$ and $n=N$.

If the surface receptor concentration is constant, the continuum limit after adiabatic elimination of fast variables is described by

$$\partial_t\lambda = \partial_x(D(\lambda)\partial_x\lambda) - k(\lambda)\lambda, \quad (11)$$

where the effective diffusion coefficient $D(\lambda)$ in the absence of extracellular diffusion (for $D_0=0$) and the effective degradation rate $k(\lambda)$ are given by

$$D(\lambda) = \frac{a^2 b_{\text{ext}} b_{\text{int}} k_{\text{off}} a k_{\text{on}} r C_-(\lambda)}{4A(\lambda)[2ak_{\text{on}}rk_{\text{off}}(b_{\text{ext}} + b_{\text{int}}) + b_{\text{int}}C_-(\lambda)]},$$

$$k(\lambda) = \frac{C_+(\lambda)}{ak_{\text{on}}\lambda}\left(\frac{b_{\text{deg}}b_{\text{int}}}{2b_{\text{ext}}(b_{\text{ext}} + b_{\text{int}})} + \frac{e_{\text{deg}}k_{\text{off}}}{C_-(\lambda)}\right). \quad (12)$$

In these expressions, $r=R/a$ and

$$A(\lambda) = \{-4b_{\text{ext}}(b_{\text{ext}} + b_{\text{int}})a^2k_{\text{on}}^2r\lambda + [b_{\text{int}}ak_{\text{on}}r + b_{\text{ext}}B_+(\lambda)]^2\}^{1/2},$$

$$B_\pm(\lambda) = k_{\text{off}} + ak_{\text{on}}(\lambda \pm r)$$

$$C_\pm(\lambda) = b_{\text{int}}ak_{\text{on}}r \mp A(\lambda) \pm b_{\text{ext}}B_\pm(\lambda).$$

These coefficients $D(\lambda)$ and $k(\lambda)$ are shown as a function of λ in Fig. 3(c). Their nonlinear dependence on the total ligand concentration λ is very similar to that of the coefficients $D_\lambda(\lambda,\rho)$ and $k_\lambda(\lambda,\rho)$ in Eq. (6), see Fig. 3(a).

We can describe transport by diffusion of receptor-bound ligands in the cell membrane by the same methods. We discuss this mechanism in Appendix D where we consider the case where endocytosis and recycling are unimportant. Furthermore, we have so far discussed the case where extracellular diffusion is weak (D_0 small). The opposite case in which extracellular diffusion dominates ligand transport is discussed in Appendix E.

IV. PROPERTIES OF TRANSPORT BY TRANSCYTOSIS

A. Nonlinear diffusion and degradation

Several key features of transcytosis follow directly from the general shape of the transport equations (6) and (7) and from the dependence of the transport and degradation coefficients on the ligand and receptor concentrations. First, the presence of the term $D_\rho(\lambda,\rho)\partial_x\rho$ in Eq. (6) shows that gradients of the receptor concentration induce a ligand current that is directed toward higher receptor concentrations since $D_\rho<0$. This contribution to the current comes up because the ligand affinity for a region increases with the receptor concentration in that region. For small ligand concentrations $D_\rho \sim \lambda$, which ensures that the corresponding current vanishes. Furthermore, D_λ and k_λ in Eq. (6) approach finite values for small λ. In this limit, Eq. (6) consequently becomes a linear diffusion equation with degradation. This implies that

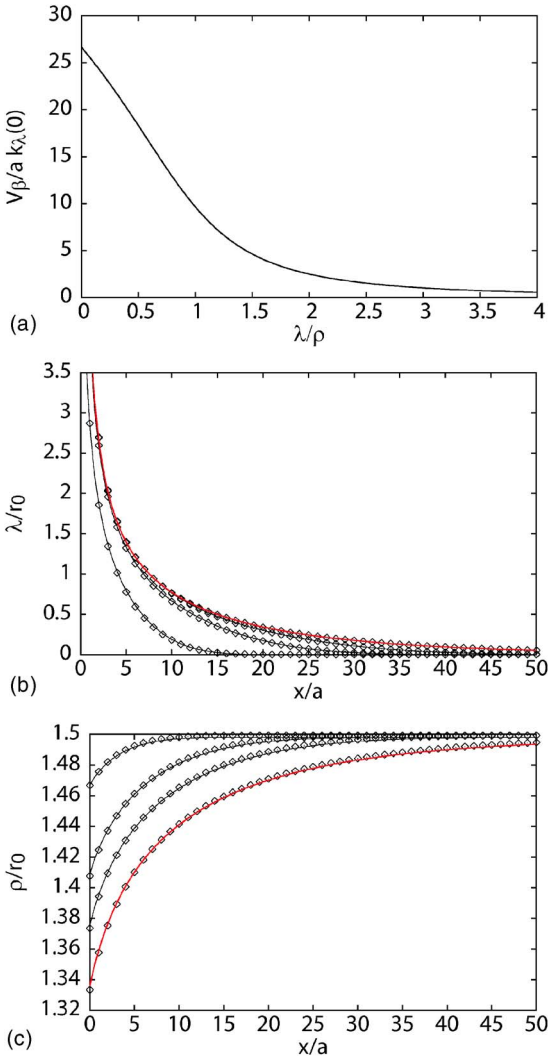

FIG. 4. (Color online) Ligand transport by transcytosis with a directional bias. (a) Drift velocity V_β from Eq. (B3) as a function of λ/ρ. (b, c) Time development of gradient formation with directional bias. Profiles of the total ligand concentration $\lambda(x,t)$ (b) and the total receptor concentration $\rho(x,t)$ (c) in the presence of a source at $x=0$ at different times $tb_{\text{deg}}=0.72, 2.16, 3.6$ during gradient formation (black lines) and in steady state (red lines). Lines indicate solutions to Eq. (9), while symbols indicate solutions to Eq. (B1) for comparison. All concentrations are normalized to the steady state value of the surface receptor concentration in the absence of ligands r_0. Initial condition: $\lambda(x)=0$ and $\rho(x)=(1+f_{\text{int}}/f_{\text{ext}})r_0$. Parameters as in Fig. 2 with $\beta=0.1$, $D_0=0$, and $j=0$ at $x/a=100$.

on large length scales and for small ligand concentrations, transcytosis is indistinguishable from passive diffusion.

In the opposite limit of large ligand concentrations λ, D_λ, and k_λ exhibit the asymptotic behavior

$$D_\lambda \simeq D_0 + c_1(\rho)\lambda^{-2}$$

and $k_\lambda \simeq e_{\mathrm{deg}} + c_2(\rho)\lambda^{-1}$. Here D_0 is the extracellular diffusion coefficient which is approached in the limit of large λ, and we have defined $c_1(\rho) = a b_{\mathrm{ext}} f_{\mathrm{int}} k_{\mathrm{off}} \rho / 4 k_{\mathrm{on}} (b_{\mathrm{ext}} + b_{\mathrm{int}})$ and $c_2(\rho) = b_{\mathrm{deg}} b_{\mathrm{int}} \rho / (b_{\mathrm{ext}} + b_{\mathrm{int}})$. The transport coefficient

$$D_\rho \simeq -D_0 - c_1(\rho)\lambda^{-2}$$

in this limit. Interestingly, both D_λ and $|D_\rho|$ approach the value D_0. This implies that transport is dominated by extracellular diffusion for large ligand concentrations λ. This behavior results from the fact that most receptors are occupied and can consequently not participate in ligand transport by transcytosis. A maximum of D_λ can occur for intermediate values of λ as long as D_0 is smaller than a critical value, see Fig. 3(a). Similarly, there can be a minimum of D_ρ as a function of λ, see Fig. 3(b). The observation that ligand transport is most efficient at a specific ligand concentration λ is an interesting consequence of the nonlinearities of the transport process.

In the special case $D_0 = 0$, D_ρ as well as D_λ vanish in the absence of receptors, i.e., for $\rho = 0$, or if either binding or unbinding of ligands from the receptor, internalization, or externalization of occupied or free receptors is suppressed, i.e., if either one of the rates k_{on}, k_{off}, b_{int}, b_{ext}, f_{int}, or f_{ext} vanishes. This reflects that in the absence of extracellular diffusion, transport is generated by repeated internalization and externalization of ligand-bound receptors as well as ligands binding to and unbinding from surface receptors. In the limit of fast internalization or fast unbinding, the ligands are confined to the cell interior or the extracellular space, respectively, and transport is consequently hampered. Indeed for $D_0 = 0$, $D_\lambda \to 0$ if $b_{\mathrm{int}} \to \infty$ or if $k_{\mathrm{off}} \to \infty$. We discuss other limits of our description in Appendix C.

Similarly, if transcytosis has a directional bias, the effective drift velocity V_β vanishes if either ρ, k_{on}, k_{off}, b_{int}, b_{ext}, f_{int}, or f_{ext} is zero and also for $b_{\mathrm{int}} \to \infty$ or $k_{\mathrm{off}} \to \infty$. Moreover, the drift velocity V_β is independent of D_0. For small λ, V_β adopts a finite value. $|V_\beta|$ is a monotonically decreasing function of λ and, in the limit of large λ, V_β vanishes as $V_\beta \simeq c_3(\rho)\lambda^{-2}$, with $c_3(\rho) = \beta b_{\mathrm{ext}} f_{\mathrm{int}} k_{\mathrm{off}} \rho / [(b_{\mathrm{ext}} + b_{\mathrm{int}}) k_{\mathrm{on}}]$, see Fig. 4(a). The fact that V_β vanishes asymptotically for large λ again reflects that transport is mediated by receptors which are only present in limited numbers.

B. Steady state concentration profile

We now calculate the steady state ligand profile formed in the half-space $x \geqslant 0$ in the presence of a source which is located at $x < 0$. In the steady state, Eq. (7) with the condition $\partial_t \rho = 0$ yields a relation $\rho(x) = \rho_s(\lambda(x))$ between the total receptor concentration ρ and the total ligand concentration λ at position x. This combined with Eq. (6) leads to the steady state equation for the ligand profile

$$\partial_x (D_s(\lambda)\partial_x \lambda) - k_s(\lambda)\lambda = 0, \tag{13}$$

with the effective diffusion coefficient in the steady state $D_s(\lambda) = D_\lambda(\lambda, \rho_s(\lambda)) + D_\rho(\lambda, \rho_s(\lambda)) d\rho_s(\lambda)/d\lambda$ and the effective degradation rate $k_s(\lambda) = k_\lambda(\lambda, \rho_s(\lambda))$. The steady state relation $\rho_s(\lambda)$ is a monotonic function of λ and converges to finite values ρ_∞ for $\lambda \to \infty$ and ρ_0 for $\lambda \to 0$. This reflects that each cell only contains a limited number of receptors and is never completely devoid of receptors. It implies that $d\rho_s/d\lambda = 0$ for large λ, so that in this limit $D_s(\lambda) \simeq D_\lambda(\lambda, \rho_\infty)$.

The steady state ligand profile $\lambda(x)$ described by Eq. (13) can be determined exactly. We rewrite Eq. (13) as

$$\partial_x j_s = -k_s(\lambda)\lambda,$$

$$\partial_x \lambda = -\frac{j_s(\lambda)}{D_s(\lambda)},$$

where the steady state current j_s is a function of $\lambda(x)$ only. This implies

$$\frac{dj_s(\lambda)}{d\lambda} = \frac{k_s(\lambda)\lambda D_s(\lambda)}{j_s(\lambda)},$$

$$\frac{dx(\lambda)}{d\lambda} = -\frac{D_s(\lambda)}{j_s(\lambda)}, \tag{14}$$

where $x(\lambda)$ is the inverse function of the steady state ligand profile $\lambda(x)$. Using Eq. (14), we find the steady state solution

$$x = -\int_{\lambda(0)}^{\lambda(x)} d\lambda' D_s(\lambda')/j_s(\lambda'), \tag{15}$$

where the steady state current is

$$j_s(\lambda) = \left(2\int_0^\lambda d\lambda' k_s(\lambda') D_s(\lambda')\lambda'\right)^{1/2}. \tag{16}$$

In the steady state, the total ligand concentration decreases monotonically with increasing distance to the source. For small λ, the ligand profile decays as $\lambda \sim \exp(-x/\xi)$ with $\xi = \sqrt{D_s(0)/k_s(0)}$. For large ligand concentrations $\lambda \gg \lambda_T$ and in the absence of free diffusion (i.e., for $D_0 = 0$), the current j_s behaves asymptotically as

$$j_s^2(\lambda) \simeq j_s(\lambda_T)^2 + 2e_{\mathrm{deg}} c_1(\rho_\infty) \ln(\lambda/\lambda_T) + 2c_1(\rho_\infty)c_2(\rho_\infty)(1/\lambda_T - 1/\lambda).$$

Here, λ_T denotes a crossover value beyond which the asymptotic behavior becomes valid. Therefore, the current diverges logarithmically as $j_s^2 \simeq 2c_1(\rho_\infty) e_{\mathrm{deg}} \ln \lambda$ for large λ and $e_{\mathrm{deg}} > 0$.

This behavior of j_s has interesting implications for the steady state ligand concentration: $\lambda(x)$ is characterized by a singularity which occurs at a position $x^* < 0$ that moves toward $x = 0$ as $\lambda(0)$ becomes large. In the vicinity of x^*, $\lambda(x)$ behaves as

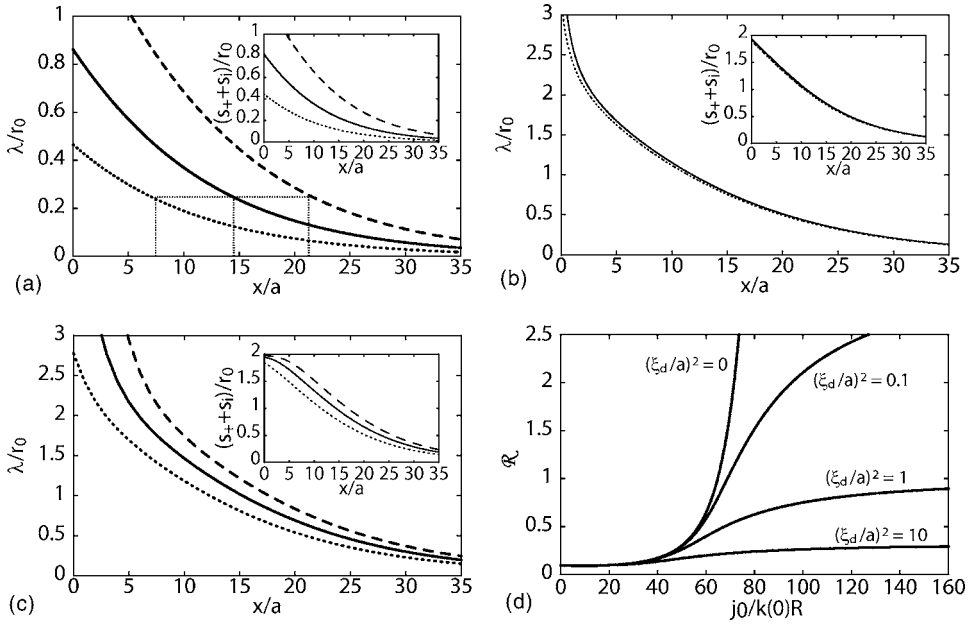

FIG. 5. Nonrobust and robust steady state gradients in our description of morphogen transport with constant surface receptor concentration given by Eq. (11). (a) Ligand profiles in the steady state for $D_0=0$ and $j_0/b_{\mathrm{deg}}R=7$ where robustness is small, $\mathcal{R}\simeq 0.1$. The profile is strongly affected by halving (dotted line) or doubling (dashed line) the ligand current of the reference state (solid line). The positions of an arbitrarily chosen concentration threshold are indicated. (b) Ligand profiles in the steady state for $D_0=0$ and $j_0/b_{\mathrm{deg}}R=70$ where robustness is large, $\mathcal{R}\simeq 470$. The reference profile (solid line) is almost unaffected by halving (dotted line) or doubling (dashed line, covered by the solid line) the ligand current of the reference state. (c) Like b but with extracellular diffusion ($D_0/a^2b_{\mathrm{deg}}=50$) which reduces robustness to $\mathcal{R}\simeq 0.32$. The insets in a–c show the respective profiles of the receptor-bound ligand concentration $s_+ + s_i$ which is the biologically relevant quantity that triggers signal transduction in the cells. (d) Robustness $\mathcal{R}$ of steady state ligand profiles as a function of the ligand current j_0 from the source for different values of the ratio of the extracellular diffusion length $\xi_d=\sqrt{D_0/e_{\mathrm{deg}}}$ and the cell size a. The description of morphogen transport with constant surface receptor approximation given by Eq. (11) was used to calculate $\mathcal{R}$. Figure modified from [20]. Parameters are $b_{\mathrm{int}}/b_{\mathrm{deg}}=b_{\mathrm{ext}}/b_{\mathrm{deg}}=3\times 10^3$, $k_{\mathrm{on}}ar/b_{\mathrm{deg}}=1.1\times 10^4$, $e_{\mathrm{deg}}/b_{\mathrm{deg}}=5$, and $k_{\mathrm{off}}/b_{\mathrm{deg}}=7\times 10^2$.

$$\lambda \sim (x-x^*)^{-1}[-\ln(x-x^*)]^{-1/2}. \tag{17}$$

Note, that the case $e_{\mathrm{deg}}=0$ has to be discussed separately. In this case, the current reaches for large λ a finite maximal value $j_{\max}$ and the steady state profile diverges as

$$\lambda \simeq c_1(\rho_\infty)/(x-x^*)j_{\max}. \tag{18}$$

If extracellular diffusion is present, i.e., if $D_0>0$, $D_s(\lambda)$ in Eq. (13) changes its asymptotic behavior to $D_s\simeq c_1(\rho_\infty)/\lambda^2+D_0$. For large $\lambda>\lambda_D$ with $\lambda_D\simeq[c_1(\rho_\infty)/D_0]^{1/2}$, Eq. (13) becomes linear and the steady state solution decays exponentially on a length scale $\xi_d=\sqrt{D_0/e_{\mathrm{deg}}}$. The nonlinear behavior described by Eqs. (17) and (18) is thus valid for $\lambda_T<\lambda<\lambda_D$.

C. Robustness of morphogen gradients

To study the robustness of morphogen gradients with respect to changes of the morphogen secretion rate, we consider the response of the steady state gradient to changes of j_0. We define the following dimensionless measure of robustness:

$$\mathcal{R}(j_0,\lambda)=a[j_0\partial_{j_0}x(\lambda)]^{-1}, \tag{19}$$

where $x(\lambda)$ is the position at which the steady state ligand profile attains the concentration λ. Here, a robustness of $\mathcal{R}(\lambda)=1$ implies that under a 100% increase of j_0 the position at which the ligand profile attains the fixed value λ is displaced by about one cell diameter a, see Fig. 5. Thus for $\mathcal{R}(\lambda)\geqslant 1$, the shift of the position x where the ligand concentration has the value λ cannot be detected by the cells in the target tissue even under significant changes of j_0.

In the absence of extracellular diffusion, the singular behavior (17) of the steady state profile near $x=x^*$ has remarkable consequences for the robustness of gradient formation. Using the robustness $\mathcal{R}$ defined in Eq. (19), we see from Eq. (15) that $\mathcal{R}$ is independent of λ. For steady state equations of the general form (13), the robustness can be calculated as

$$\mathcal{R}=a(j_0\partial_{j_0}x)^{-1}=a\partial_{\lambda_0}j_0/D_s(\lambda_0)=ak_s(\lambda_0)\lambda_0/j_0, \tag{20}$$

where $\lambda_0=\lambda(x=0)$ and Eqs. (15) and (16) have been used. The robustness is thus completely determined by the ratio of the effective degradation rate and the ligand current at $x=0$ and does not depend on λ, i.e., it is the same at all positions x of the concentration gradient $\lambda(x)$. High degradation rates and small currents lead to a robust gradient. Using the asymptotic behavior of the steady state profile for $D_0=0$, we find that the robustness increases rapidly for large currents j_0 as $\mathcal{R}\sim j_0^{-1}e^{j_0^2/j_c^2}$ with $j_c^2=1/2c_1(\rho_\infty)e_{\mathrm{deg}}$. For small j_0, $\mathcal{R}\simeq a/\xi$ becomes constant. In Figs. 5(a) and 5(b), we illustrate

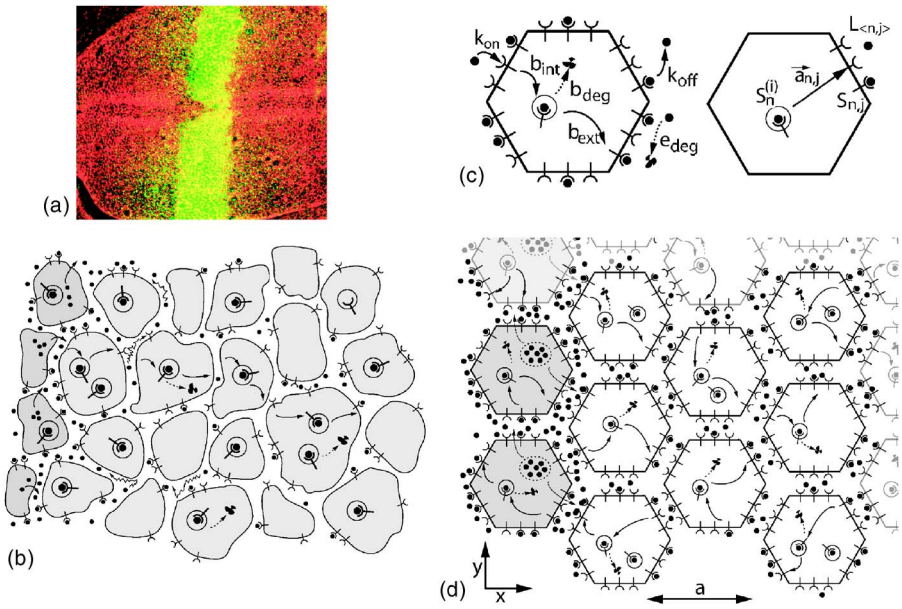

FIG. 6. (Color online) Ligand transport in two dimensions. (a) Tissue in the region of the wing disk where the Dpp gradient forms. Cell membranes are labeled in red, the morphogen Dpp is shown in green. (b) Schematic of this tissue. Source cells which produce ligands are shown in darker gray, the cells in the target tissue in light gray. (c) The rates for the various cellular processes are denoted as in one dimension, see Fig. 1. For the triangular lattice with hexagonal cells which we use here, receptor bound ligands can be present on the six edges of each cell and inside the cells. The concentration of the receptor-bound ligands on edge j of cell n is denoted $S_{n,j}$, that inside cell n is termed $S_n^{(\mathrm{i})}$. Free ligands exist in the gaps between two cell surfaces. Their concentration in gap $\langle n,j\rangle$ which is located adjacent to edge j of cell n is denoted $L_{\langle n,j\rangle}$. (d) Triangular lattice structure with hexagonal cells used in our discrete theoretical description of ligand transport in two dimensions. This lattice structure approximates the situation shown in b. The source cells which are shown in darker gray secrete ligands into the extracellular spaces surrounding them. The cell diameter is a.

the behavior of the robustness of steady state gradients for a small and a large value of j_0.

The situation is different if free diffusion in the extracellular space is present. As discussed in the previous section, the singularity in the steady state solution disappears for $D_0>0$. As a result of this, the robustness approaches a finite value $\mathcal{R}_{\max}=a/\xi_d$ as $j_0\to\infty$. In Fig. 5(d), $\mathcal{R}(j_0)$ is shown for different values of ξ_d/a and Fig. 5(c) shows an example for the effect of the presence of extracellular diffusion on the robustness of the gradient.

In summary, we find that morphogen gradients can be extremely robust to changes in the morphogen secretion rate of the source cells if transport is dominated by transcytosis. The presence of extracellular diffusion reduces this robustness that is completely lost when extracellular diffusion is the dominant transport mechanism.

V. MORPHOGEN TRANSPORT IN TWO DIMENSIONS

A. Ligand kinetics on the cellular scale

The theoretical framework introduced in the previous sections can be extended to higher dimensions. Considering a two-dimensional geometry, we represent the cells in the tissue on the sites of a discrete lattice. The tissue geometry of the wing disk can be captured by an irregular tiling of the plane, see Figs. 6(a) and 6(b). For simplicity, however, we use a triangular lattice with N hexagonal cells in our description, see Fig. 6(d). Each hexagonal cell $n=1,\ldots,N$ has J edges (n,j) with $j=1,\ldots,J$ ($J=6$ for a triangular lattice) along which it faces a uniquely defined neighboring cell n' at its edge (n',j'), see Fig. 6(c). The space between these two facing edges of the neighboring cells is denoted by the symbol $\langle n,j\rangle$ with the property $\langle n,j\rangle=\langle n',j'\rangle$.

To keep our notation simple, we first discuss the case of constant surface receptor concentration, see Sec. III D. Assuming that there is no directional bias of ligand transport, the externalization of the ligand-receptor complexes can occur on all surfaces of the cell with equal probability. The equations for the ligand kinetics corresponding to Eq. (10) on a lattice are

$$\frac{d}{dt}L_{\langle n,j\rangle}=k_{\mathrm{off}}(S_{n,j}+S_{n',j'})-\frac{Jk_{\mathrm{on}}}{2}\left(\frac{2R}{J}-S_{n,j}-S_{n',j'}\right)L_{\langle n,j\rangle}-e_{\mathrm{deg}}L_{\langle n,j\rangle},$$

$$\frac{d}{dt}S_{n,j}=\frac{b_{\mathrm{ext}}}{J}S_n^{(\mathrm{i})}-(b_{\mathrm{int}}+k_{\mathrm{off}})S_{n,j}+\frac{Jk_{\mathrm{on}}}{2}\left(\frac{R}{J}-S_{n,j}\right)L_{(n,j)},$$

$$\frac{d}{dt}S_n^{(\mathrm{i})}=-b_{\mathrm{ext}}S_n^{(\mathrm{i})}+b_{\mathrm{int}}\sum_{j=1}^{J}S_{n,j}-b_{\mathrm{deg}}S_n^{(\mathrm{i})},\qquad(21)$$

where $S_n^{(\mathrm{i})}$ is the internal bound ligand concentration in cell n, $S_{n,j}$ the surface bound ligand concentration on edge j of cell n, and $L_{\langle n,j\rangle}$ the free ligand concentration in the extracellular space $\langle n,j\rangle$ which is located between the two adjacent cells n

and n' and the edges (n,j) and (n',j'), see Figs. 6(c) and 6(d). In Eq. (21), we have for simplicity neglected extracellular diffusion which would couple the concentration $L_{\langle n,j\rangle}$ to the one on neighboring sites. At the boundaries of the lattice, the equation for $\frac{d}{dt}L_{\langle n,j\rangle}$ in (21) takes into account ligand influx analogously to the one-dimensional situation, see Eqs. (3) and (4).

B. Transport equations on larger scales

The effective behavior of ligand transport as described by Eq. (21) exhibits anisotropy on large scales due to the anisotropic lattice structure. We consider for simplicity an isotropic continuum limit. This simplification is motivated by the irregular arrangement of cells in a tissue which does not exhibit lattice anisotropies.

In the isotropic case, the continuum limit describing transport by transcytosis in two dimensions is of the general form

$$\partial_t \lambda = \nabla \cdot [D^{2d}(\lambda)\, \nabla\, \lambda] - k^{2d}(\lambda)\lambda. \tag{22}$$

The effective coefficients $D^{2d}(\lambda)$ and $k^{2d}(\lambda)$ in Eq. (22) are in general different from those in the one-dimensional case (12). In order to determine values for the coefficients $D^{2d}(\lambda)$ and $k^{2d}(\lambda)$ we first consider concentration profiles which vary only along one symmetry axis of the lattice given by the x axis in Fig. 6(d). In this situation the problem can be represented on a one-dimensional lattice similar to the one-dimensional chain discussed above. We thus determined $D^{2d}(\lambda)$ and $k^{2d}(\lambda)$ along this lattice axis using our one-dimensional approach. Lattice symmetry implies that these coefficients apply to three different lattice axes. In our isotropic simplification, we assume that they apply to all directions. From this argument, we find the same effective degradation rate $k^{2d}(\lambda)=k(\lambda)$ as in one dimension, see Eq. (12). The effective diffusion coefficient changes by a factor of $2/3$: $D^{2d}(\lambda)=(2/3)D(\lambda)$.

By the same considerations, the more general description with receptor kinetics introduced in one dimension in Eqs. (6) and (7) generalizes in two dimensions to

$$\partial_t \lambda = \nabla \cdot [D_\lambda^{2d}(\lambda,\rho)\, \nabla\, \lambda + D_\rho^{2d}(\lambda,\rho)\, \nabla\, \rho] - k_\lambda^{2d}(\lambda,\rho)\lambda,$$

$$\partial_t \rho = \nu_{\mathrm{sys}}^{2d}(\lambda,\rho) - k_\rho^{2d}(\lambda,\rho)\rho.$$

Here the coefficients $D_\lambda^{2d}(\lambda,\rho)$, $D_\rho^{2d}(\lambda,\rho)$, $k_\lambda^{2d}(\lambda,\rho)$, and $k_\rho^{2d}(\lambda,\rho)$ are in general modified due to the lattice geometry. For a triangular lattice $D_\lambda^{2d}(\lambda,\rho)=(2/3)D_\lambda(\lambda,\rho)$ and $D_\rho^{2d}(\lambda,\rho)=(2/3)D_\rho(\lambda,\rho)$. The degradation rates k_λ^{2d} and k_ρ^{2d} are identical to those in the one-dimensional case. Finally, the rate of receptor synthesis $\nu_{\mathrm{syn}}^{2d}=\nu_{\mathrm{syn}}/a$ is the same as in one dimension, see Eq. (8), but measured in different units. At the boundary line at $x=0$, the ligand source is described by a current $j_0=\nu/a$ across this boundary line.

We have compared solutions of the effective continuum equation in two dimensions (22) to those of the discrete description on a triangular lattice (21). Here, the ligand source located at $x<0$ extends along the y direction. This setup is translation invariant along this direction if no inhomogeneities are present in the tissue. In this situation, the solutions of the discrete and continuum descriptions are in good agreement. In order to test the validity of the continuum description for a case that is not translation invariant along the y direction, we compared the solutions of Eq. (22) for a geometry in which a rectangular region which the ligand cannot enter is present in the tissue to solutions of Eq. (21) where such a rectangular region is approximated, see Fig. 7. In the discrete description, we imposed this constraint by setting $b_{\mathrm{int}}=0$ in this region. In the continuum description (22), this corresponds to $D^{2d}=0$ within this region which we realized by imposing a zero flux boundary condition ($j=0$) at its border. As in one dimension, the continuum description is appropriate as long as the degradation rates and the hopping rate D_0/a^2 which describes extracellular diffusion remain small.

VI. DISCUSSION

In this article, we have first presented a description of morphogen transport in which cells are discrete entities. This description is based on key processes like the diffusion of morphogens in the extracellular space, binding and unbinding of the morphogens to and from receptor molecules that are located on the cell surfaces, internalization of these receptor-ligand complexes into the cell and their subsequent recycling, as well as degradation of external and internalized ligands, see Fig. 1. Moreover, the production and intracellular trafficking of free receptor molecules by the cells is included. We have derived effective nonlinear transport equations (6) and (7) for the total morphogen concentration and the total receptor concentration which describe transport by transcytosis on larger length scales. The effective diffusion coefficient and the effective degradation rate in these equations are concentration dependent. If transcytosis has a directional bias, an additional drift term appears in the transport equations.

Other mechanisms of ligand transport can be effectively described by equations (6) and (7). The effective transport coefficients can be derived from a detailed description of any particular transport mechanism. As an example for this, we have discussed a model of morphogen transport where transport occurs via diffusion of ligands bound to carrier molecules in the cell membrane [11,26], see Appendix D.

Our theoretical discription of morphogen transport captures the key processes that are relevant for ligand transport and ligand-receptor interactions in multicellular epithelia such as the wing disk. We used a simplified description of these processes and neglected several aspects that could play a role. For example, we did not account for cell divisions and tissue growth in our description [27]. More importantly, the presence of different receptor types which is quite common for signaling molecules of the TGF-β superfamily like Dpp was neglected in our description. These receptors typically form dimers or other complexes and, in general, the affinity of the ligand is different for the different receptor types and complexes. The trafficking of ligand-receptor pairs inside the cell is a very complex process that is only crudely captured in our description by a few parameters.

Our coarse-graining procedure starts from a discrete cellular representation and allows us to obtain effective trans-

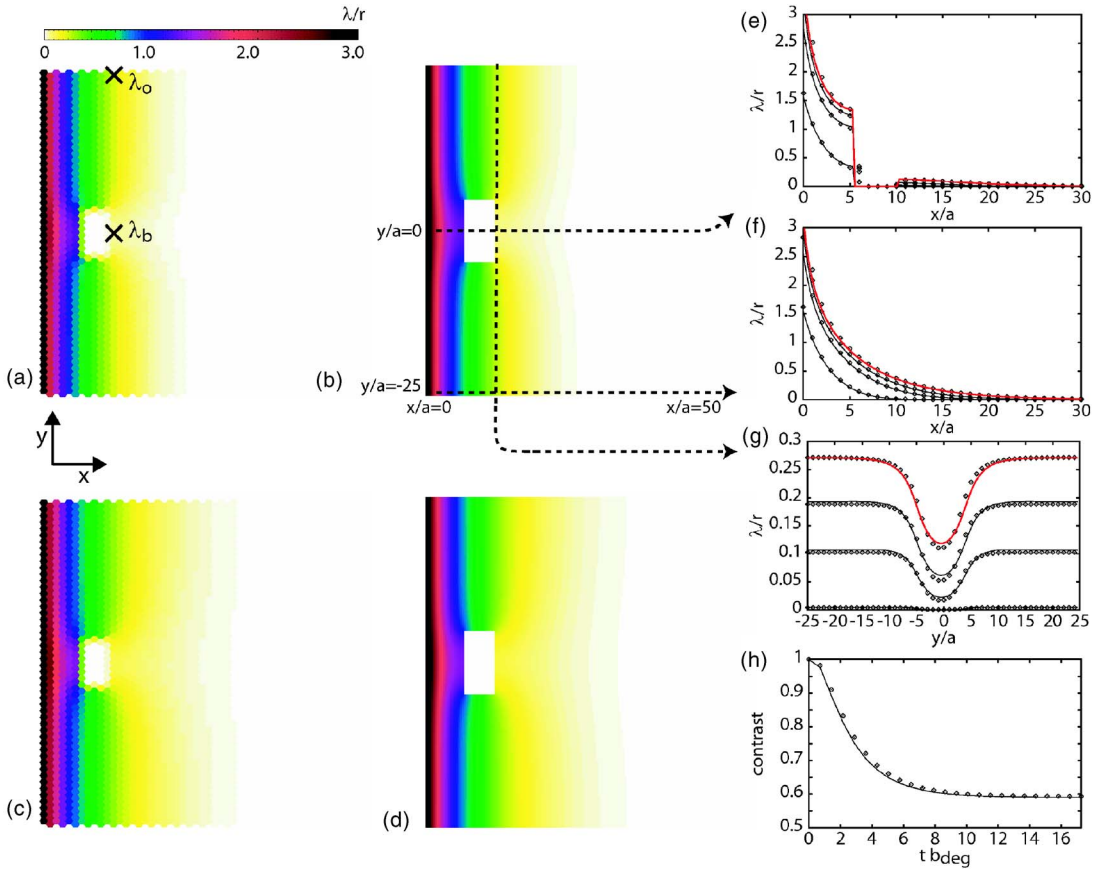

FIG. 7. (Color online) Time development of ligand densities $\lambda(\vec{x},t)$ in two dimensions. The solution to the continuum transport equation (22) is compared to that of the discrete description given by Eq. (21) in the presence of a region which the ligand cannot enter located at $6 \leqslant x/a \leqslant 11$ and $-4 \leqslant y/a \leqslant 4$. In the discrete description, this is realized by setting b_{int} to zero in the region. In the continuum description, zero flux boundary conditions are imposed on the outlining edge of the region. (a–d) Two-dimensional ligand profiles at $tb_{\mathrm{deg}}=3.6$ (a,b) and at $tb_{\mathrm{deg}}=17.3$ which is close to the steady state (c,d). These profiles were obtained by solving the discrete (a,c) and continuum description (b,d), respectively. The rectangular region which the ligand cannot enter appears in white. It appears smaller in a and c than in b and d because in the discrete description, ligands can still bind to surface receptors on the cells located at the edge of the region so that $\lambda > 0$ for these cells. (e–g) Profiles of $\lambda(\vec{x},t)$ along the slices indicated in b at $tb_{\mathrm{deg}}=0.72, 2.16, 3.6$ (black lines) and in steady state (red lines). Lines indicate solutions to Eq. (22), while symbols indicate solutions to Eq. (21) for comparison. (h) Contrast of the depletion of $\lambda(\vec{x},t)$ shown in g. The contrast is defined as $c(t)=1-\lambda_b(t)/\lambda_o(t)$ where $\lambda_b(t)$ and $\lambda_o(t)$ are the total ligand concentration at the locations shown by the crosses in a, i.e., directly behind the clone and far away from it, respectively. Initial condition: $\lambda(\vec{x})=0$. Parameters as in Fig. 2 with $D_0=0$, $j_0/b_{\mathrm{deg}}ar=25/3$ at $x=0$, $j=0$ at $y/a=\pm 25$ and at $x/a=50$.

port equations in a continuum limit. This provides a theoretical framework for a quantitative analysis of the spreading and trafficking of signaling molecules in and between cells. Using this approach one can relate experimental data obtained at different scales ranging from the cell to the tissue level. For example, the situation shown in Fig. 7 mimics recent experiments done in the Drosophila wing disk in which endocytosis is blocked in patches of cells in the tissue (see Sec. II) [6]. The calculation results shown in Fig. 7 are consistent with the experimental data obtained in these shibire clone experiments [6]. They show a ligand depletion of decreasing relative magnitude ("contrast") behind the clone region as it is observed experimentally, see Fig. 7(h). Note, that the clone region itself is devoid of ligands which is also seen experimentally and is evidence for a transport mechanism via transcytosis [13].

Transport processes of signaling molecules in tissues show many features in common which are captured by our description. Our study highlights some general properties of these systems such as the robustness of gradients which are largely independent of parameter values and molecular details. We expect that such general features can play an important role in very different biological signaling systems.

APPENDIX A: DERIVATION OF THE EFFECTIVE TRANSPORT EQUATIONS IN ONE DIMENSION

To perform a continuum limit of Eq. (1), we introduce the densities $l(t,x)$, $r^{(\mathrm{l/r})}(t,x)$, $r_i(t,x)$, $s^{(\mathrm{l/r})}(t,x)$, and $s_i(t,x)$, such that $x=na$, $L_n(t)/a=l(t,x)$, $R_n^{(\mathrm{l})}(t)/a=r^{(\mathrm{l})}(t,x)$, $R_n^{(\mathrm{r})}(t)/a=r^{(\mathrm{r})}(t,x)$, $R_n^{(\mathrm{i})}(t)/a=r_i(t,x)$, $S_n^{(\mathrm{l})}(t)/a=s^{(\mathrm{l})}(t,x)$, $S_n^{(\mathrm{r})}(t)/a=s^{(\mathrm{r})}(t,x)$, and $S_n^{(\mathrm{i})}(t)/a=s_i(t,x)$. Kinetic equations for these are obtained by replacing the discrete densities $R_n^{(\mathrm{i})}$, $R_n^{(\mathrm{l/r})}$, $S_n^{(\mathrm{i})}$, $S_n^{(\mathrm{l/r})}$, and L_n in Eq. (1) with the continuum densities r_i, $r^{(\mathrm{l/r})}$, s_i, $s^{(\mathrm{l/r})}$, and l. The spatial separation of the quantities defined

on the lattice as indicated in Fig. 1 is taken into account by including terms up to second order in a power series expansion in x. We also change variables to $r_{\pm}(t,x) = r^{(l)}(t,x) \pm r^{(r)}(t,x)$ and $s_{\pm}(t,x) = s^{(l)}(t,x) \pm s^{(r)}(t,x)$ so that r_+ and s_+ measure the total free and ligand bound surface receptor concentrations per cell and r_- and s_- the polarization of these concentrations on the cell surface, respectively. This yields the continuum equations

$$\partial_t l = k_{\text{off}} s_+ - (a k_{\text{on}} r_+ + e_{\text{deg}}) l - \frac{a b^2 k_{\text{on}}}{8} l \partial_x^2 r_+ + \frac{b^2 k_{\text{off}}}{8} \partial_x^2 s_+ + D_0 \partial_x^2 l - \frac{a b k_{\text{on}}}{2} l \partial_x r_- + \frac{b k_{\text{off}}}{2} \partial_x s_-,$$

$$\partial_t s_+ = a k_{\text{on}} l r_+ + b_{\text{ext}} s_i - (b_{\text{int}} + k_{\text{off}}) s_+ + \frac{a b^2 k_{\text{on}}}{8} r_+ \partial_x^2 l + \frac{(a-b)^2 b_{\text{ext}}}{8} \partial_x^2 s_i - \frac{a b k_{\text{on}}}{2} r_- \partial_x l,$$

$$\partial_t s_i = -(b_{\text{ext}} + b_{\text{deg}}) s_i + b_{\text{int}} s_+ + \frac{(a-b)^2 b_{\text{int}}}{8} \partial_x^2 s_+ - \frac{(a-b) b_{\text{int}}}{2} \partial_x s_-,$$

$$\partial_t s_- = a k_{\text{on}} l r_- - (b_{\text{int}} + k_{\text{off}}) s_- + \frac{a b^2 k_{\text{on}}}{8} r_- \partial_x^2 l - \frac{a b k_{\text{on}}}{2} r_+ \partial_x l + \frac{(a-b) b_{\text{ext}}}{2} \partial_x s_i,$$

$$\partial_t r_+ = \frac{f_{\text{syn}}}{a} + f_{\text{ext}} r_i - f_{\text{int}} r_+ - a k_{\text{on}} l r_+ + k_{\text{off}} s_+ - \frac{a b^2 k_{\text{on}}}{8} r_+ \partial_x^2 l + \frac{(a-b)^2 f_{\text{ext}}}{8} \partial_x^2 r_i + \frac{a b k_{\text{on}}}{2} r_- \partial_x l,$$

$$\partial_t r_i = -(f_{\text{ext}} + f_{\text{deg}}) r_i + f_{\text{int}} r_+ + \frac{(a-b)^2 f_{\text{int}}}{8} \partial_x^2 r_+ - \frac{(a-b) f_{\text{int}}}{2} \partial_x r_-,$$

$$\partial_t r_- = -f_{\text{int}} r_- - a k_{\text{on}} l r_- + k_{\text{off}} s_- - \frac{a b^2 k_{\text{on}}}{8} r_- \partial_x^2 l + \frac{a b k_{\text{on}}}{2} r_+ \partial_x l + \frac{(a-b) f_{\text{ext}}}{2} \partial_x r_i. \tag{A1}$$

Here, it is reasonable to neglect derivatives of higher order with respect to x because the most important contribution to ligand transport on large length scales comes from the second derivative terms. This is due to the fact that first derivative terms must not appear in an effective transport equation because of the mirror symmetry of the original description.

In the absence of degradation and production, there are two conserved quantities in the system, namely the total ligand number and the total receptor number. Indeed, the kinetic equation for the total ligand density $\lambda = l + s_i + s_+$ that follows from Eq. (A1) can be written as a continuity equation with sink term

$$\partial_t \lambda = -\partial_x j - b_{\text{deg}} s_i - e_{\text{deg}} l. \tag{A2}$$

Here, the total ligand current is

$$j = \frac{a b k_{\text{on}}}{2} l r_- + \frac{(a-b) b_{\text{int}}}{2} s_- - \frac{b k_{\text{off}}}{2} s_- - \frac{a b^2 k_{\text{on}}}{8} (r_+ \partial_x l - l \partial_x r_+) - \frac{(a-b)^2 b_{\text{ext}}}{8} \partial_x s_i - \frac{(a-b)^2 b_{\text{int}} + b^2 k_{\text{off}}}{8} \partial_x s_+ - D_0 \partial_x l. \tag{A3}$$

Note, that the terms involving r_- and s_- appear directly whereas all other terms are proportional to derivatives of r_+, s_+, s_i, or l. The kinetics of the total receptor density $\rho = r_i + r_+ + s_i + s_+$ is given by another continuity equation with source and sink terms:

$$\partial_t \rho = -\partial_x j_\rho + \frac{f_{\text{syn}}}{a} - f_{\text{deg}} r_i - b_{\text{deg}} s_i \tag{A4}$$

with the total receptor current

$$j_\rho = \frac{(a-b)}{2} (f_{\text{int}} r_- + b_{\text{int}} s_-) - \frac{(a-b)^2}{8} (f_{\text{ext}} \partial_x r_i + f_{\text{int}} \partial_x r_+ + b_{\text{ext}} \partial_x s_i + b_{\text{int}} \partial_x s_+). \tag{A5}$$

The individual terms of the currents j and j_ρ are difficult to interpret. However, it will become clear below that the terms in j_ρ do not give rise to transport over large distances whereas this is the case for the terms in j.

The equations (A2) and (A4) have the unpleasant property that they relate the time development of λ and ρ to that of all the individual quantities $l, s_i, s_\pm, r_i, r_\pm$ whose time development is given by the set of coupled partial differential equations (A1). It would be better if the kinetics of λ and ρ could be described by equations which only involve these two quantities. This can be achieved by exploiting a separation of time scales.

As discussed in the main text, the relaxation time scale τ_a for the kinetics in one cell is much smaller than the time scale τ_{ξ_D} for ligand transport on a large length scale ξ_D on which the ligand profile develops. As we are interested in the behavior on large length scales in the continuum description, we exploit $\tau_a \ll \tau_{\xi_D}$ by making an adiabatic approximation in which the system equilibrates infinitely fast locally. This is done by setting all time derivatives in Eq. (A1) to zero and neglecting the second derivative terms. The resulting equations provide five relations between the seven variables $l, r_i, r_\pm, s_i, s_\pm$. Here, we also assume that the production and degradation rates are small compared to the other rates. Formally, this corresponds to setting $b_{\text{deg}} = e_{\text{deg}} = f_{\text{deg}} = f_{\text{syn}} = 0$. This procedure yields the relations (5).

Note, that we have kept the first derivative terms for r_- and s_- in Eq. (5). This is done to retain all second derivative

terms when inserting Eq. (5) into Eqs. (A2)–(A5). Using Eq. (5), one can express l, r_i, r_-, s_i, s_- in terms of r_+ and s_+ and spatial derivatives thereof. Finally, r_+ and s_+ can be expressed in terms of $\rho = r_i + r_+ + s_i + s_+$ and $\lambda = l + s_i + s_+$. Mathematically, there exist two solutions for $s_+(\lambda,\rho)$ and $r_+(\lambda,\rho)$ but only one of them satisfies the physical requirement that $s_+(\lambda=0,\rho)=0$ and $r_+(\lambda,\rho=0)=0$. Thus, we can uniquely express l, r_i, $r_\pm$, s_i, and $s_\pm$ in terms of λ and ρ in the adiabatic approximation.

Using these expressions, it is straightforward to cast Eqs. (A2)–(A5) into the two coupled partial differential equations (6) and (7). The explicit expressions for the transport and degradation coefficients in this one-dimensional description of morphogen transport are

$$\begin{aligned}
D_\lambda(\lambda,\rho) = &- a^3 b_{\mathrm{ext}} b_{\mathrm{int}} (b_{\mathrm{ext}} + b_{\mathrm{int}}) {f_{\mathrm{ext}}}^2 f_{\mathrm{int}} k_{\mathrm{off}} k_{\mathrm{on}} \rho [-2 b_{\mathrm{int}} [b_{\mathrm{ext}} (f_{\mathrm{ext}} + f_{\mathrm{int}}) k_{\mathrm{off}} + a (b_{\mathrm{ext}} + b_{\mathrm{int}}) f_{\mathrm{ext}} k_{\mathrm{on}} \lambda]^2 \\
&+ 2A(\lambda,\rho)(-\{b_{\mathrm{int}} f_{\mathrm{ext}} [2 f_{\mathrm{int}} (b_{\mathrm{int}} + k_{\mathrm{off}}) + a b_{\mathrm{int}} k_{\mathrm{on}} \lambda]\} + b_{\mathrm{ext}} \{-2 f_{\mathrm{ext}} f_{\mathrm{int}} k_{\mathrm{off}} + b_{\mathrm{int}} [f_{\mathrm{int}} k_{\mathrm{off}} + f_{\mathrm{ext}} (-2 f_{\mathrm{int}} + k_{\mathrm{off}} - a k_{\mathrm{on}} \lambda)]\}) \\
&+ 2a b_{\mathrm{int}} (b_{\mathrm{ext}} + b_{\mathrm{int}}) f_{\mathrm{ext}} k_{\mathrm{on}} [A(\lambda,\rho) - 2 b_{\mathrm{ext}} (f_{\mathrm{ext}} + f_{\mathrm{int}}) k_{\mathrm{off}} + 2a (b_{\mathrm{ext}} + b_{\mathrm{int}}) f_{\mathrm{ext}} k_{\mathrm{on}} \lambda] \rho - 2a^2 b_{\mathrm{int}} (b_{\mathrm{ext}} + b_{\mathrm{int}})^2 {f_{\mathrm{ext}}}^2 {k_{\mathrm{on}}}^2 \rho^2]^{-1} \\
&+ 2 D_0 a b_{\mathrm{ext}} (b_{\mathrm{ext}} + b_{\mathrm{int}}) f_{\mathrm{ext}} (f_{\mathrm{ext}} + f_{\mathrm{int}}) k_{\mathrm{off}} k_{\mathrm{on}} \rho [A(\lambda,\rho)(A(\lambda,\rho) - b_{\mathrm{ext}} \{f_{\mathrm{int}} k_{\mathrm{off}} + f_{\mathrm{ext}} [k_{\mathrm{off}} + a k_{\mathrm{on}} (\lambda - \rho)]\} \\
&+ a b_{\mathrm{int}} f_{\mathrm{ext}} k_{\mathrm{on}} (\rho - \lambda))]^{-1},
\end{aligned}$$

$$\begin{aligned}
D_\rho(\lambda,\rho) = &\, a^4 b_{\mathrm{ext}} b_{\mathrm{int}} (b_{\mathrm{ext}} + b_{\mathrm{int}}) {f_{\mathrm{ext}}}^2 f_{\mathrm{int}} k_{\mathrm{off}} {k_{\mathrm{on}}}^2 \lambda \rho [2(\{-[f_{\mathrm{int}} (b_{\mathrm{int}} + k_{\mathrm{off}})] - a b_{\mathrm{int}} k_{\mathrm{on}} \lambda\} [b_{\mathrm{ext}} (f_{\mathrm{ext}} + f_{\mathrm{int}}) k_{\mathrm{off}} + a (b_{\mathrm{ext}} + b_{\mathrm{int}}) f_{\mathrm{ext}} k_{\mathrm{on}} \lambda] \\
&\times [A(\lambda,\rho) + b_{\mathrm{ext}} (f_{\mathrm{ext}} + f_{\mathrm{int}}) k_{\mathrm{off}} + a (b_{\mathrm{ext}} + b_{\mathrm{int}}) f_{\mathrm{ext}} k_{\mathrm{on}} \lambda] + a (b_{\mathrm{ext}} + b_{\mathrm{int}}) f_{\mathrm{ext}} k_{\mathrm{on}} (-[A(\lambda,\rho) f_{\mathrm{int}} (b_{\mathrm{int}} + k_{\mathrm{off}})] + a A(\lambda,\rho) b_{\mathrm{int}} k_{\mathrm{on}} \lambda \\
&+ 2[f_{\mathrm{int}} (b_{\mathrm{int}} + k_{\mathrm{off}}) + a b_{\mathrm{int}} k_{\mathrm{on}} \lambda] \{-[b_{\mathrm{ext}} (f_{\mathrm{ext}} + f_{\mathrm{int}}) k_{\mathrm{off}}] + a (b_{\mathrm{ext}} + b_{\mathrm{int}}) f_{\mathrm{ext}} k_{\mathrm{on}} \lambda\}) \rho - a^2 (b_{\mathrm{ext}} + b_{\mathrm{int}})^2 {f_{\mathrm{ext}}}^2 {k_{\mathrm{on}}}^2 \\
&\times [f_{\mathrm{int}} (b_{\mathrm{int}} + k_{\mathrm{off}}) + a b_{\mathrm{int}} k_{\mathrm{on}} \lambda] \rho^2)]^{-1} + 2 D_0 b_{\mathrm{ext}} (f_{\mathrm{ext}} + f_{\mathrm{int}}) k_{\mathrm{off}} [([(f_{\mathrm{ext}} + f_{\mathrm{int}}) k_{\mathrm{off}} + a f_{\mathrm{ext}} k_{\mathrm{on}} \lambda]^2 + a f_{\mathrm{ext}} k_{\mathrm{on}} [(f_{\mathrm{ext}} + f_{\mathrm{int}}) k_{\mathrm{off}} \\
&- a f_{\mathrm{ext}} k_{\mathrm{on}} \lambda] \rho) {b_{\mathrm{ext}}}^2 - A(\lambda,\rho) [(f_{\mathrm{ext}} + f_{\mathrm{int}}) k_{\mathrm{off}} + a f_{\mathrm{ext}} k_{\mathrm{on}} \lambda] b_{\mathrm{ext}} + a b_{\mathrm{int}} f_{\mathrm{ext}} k_{\mathrm{on}} [2 f_{\mathrm{ext}} \lambda (k_{\mathrm{off}} + a k_{\mathrm{on}} \lambda) + f_{\mathrm{ext}} (k_{\mathrm{off}} - 2 a k_{\mathrm{on}} \lambda) \rho \\
&+ f_{\mathrm{int}} k_{\mathrm{off}} (2\lambda + \rho)] b_{\mathrm{ext}} + a b_{\mathrm{int}} f_{\mathrm{ext}} k_{\mathrm{on}} \lambda \times [a b_{\mathrm{int}} f_{\mathrm{ext}} k_{\mathrm{on}} (\lambda - \rho) - A(\lambda,\rho)]] [A(\lambda,\rho)(A(\lambda,\rho) - b_{\mathrm{ext}} \{f_{\mathrm{int}} k_{\mathrm{off}} + f_{\mathrm{ext}} [k_{\mathrm{off}} + a k_{\mathrm{on}} (\lambda \\
&- \rho)]\} + a b_{\mathrm{int}} f_{\mathrm{ext}} k_{\mathrm{on}} (\rho - \lambda))^2]^{-1},
\end{aligned}$$

$$k_\lambda(\lambda,\rho) = [b_{\mathrm{deg}} b_{\mathrm{int}} (a b_{\mathrm{int}} f_{\mathrm{ext}} k_{\mathrm{on}} (\lambda + \rho) - A(\lambda,\rho) + b_{\mathrm{ext}} \{f_{\mathrm{int}} k_{\mathrm{off}} + f_{\mathrm{ext}} [k_{\mathrm{off}} + a k_{\mathrm{on}} (\lambda + \rho)]\})][2a (b_{\mathrm{ext}} + b_{\mathrm{int}})^2 f_{\mathrm{ext}} k_{\mathrm{on}} \lambda]^{-1}$$

$$\begin{aligned}
k_\rho(\lambda,\rho) = &(\{-[(b_{\mathrm{ext}} + b_{\mathrm{int}}) f_{\mathrm{deg}} f_{\mathrm{int}}] + b_{\mathrm{deg}} b_{\mathrm{int}} (f_{\mathrm{ext}} + f_{\mathrm{int}})\} [-A(\lambda,\rho) + b_{\mathrm{ext}} (f_{\mathrm{ext}} + f_{\mathrm{int}}) k_{\mathrm{off}} + a (b_{\mathrm{ext}} + b_{\mathrm{int}}) f_{\mathrm{ext}} k_{\mathrm{on}} \lambda] \\
&+ a (b_{\mathrm{ext}} + b_{\mathrm{int}}) f_{\mathrm{ext}} [(b_{\mathrm{ext}} + b_{\mathrm{int}}) f_{\mathrm{deg}} f_{\mathrm{int}} + b_{\mathrm{deg}} b_{\mathrm{int}} (f_{\mathrm{ext}} + f_{\mathrm{int}})] k_{\mathrm{on}} \rho) \times [2a (b_{\mathrm{ext}} + b_{\mathrm{int}})^2 f_{\mathrm{ext}} (f_{\mathrm{ext}} + f_{\mathrm{int}}) k_{\mathrm{on}} \rho]^{-1},
\end{aligned}$$

with

$$A(\lambda,\rho) = [(b_{\mathrm{ext}} \{f_{\mathrm{int}} k_{\mathrm{off}} + f_{\mathrm{ext}} [k_{\mathrm{off}} + a k_{\mathrm{on}} (\lambda - \rho)]\} + a b_{\mathrm{int}} f_{\mathrm{ext}} k_{\mathrm{on}} (\lambda - \rho))^2 + 4 a b_{\mathrm{ext}} (b_{\mathrm{ext}} + b_{\mathrm{int}}) f_{\mathrm{ext}} (f_{\mathrm{ext}} + f_{\mathrm{int}}) k_{\mathrm{off}} k_{\mathrm{on}} \rho]^{1/2}. \quad \text{(A6)}$$

APPENDIX B: DIRECTIONAL BIAS OF INTRACELLULAR TRAFFICKING

We study the effects of a bias in the description of transcytosis. We introduce a dimensionless parameter $-1/2 \leqslant \beta \leqslant 1/2$ which measures this bias in Eq. (1). The kinetic equations of the discrete description with bias are

$$\begin{aligned}
\frac{d}{dt} S_n^{(\mathrm{r})} &= -k_{\mathrm{off}} S_n^{(\mathrm{r})} + k_{\mathrm{on}} R_n^{(\mathrm{r})} L_n - b_{\mathrm{int}} S_n^{(\mathrm{r})} + b_{\mathrm{ext}} (1/2 + \beta) S_n^{(\mathrm{i})}, \\
\frac{d}{dt} S_n^{(\mathrm{l})} &= -k_{\mathrm{off}} S_n^{(\mathrm{l})} + k_{\mathrm{on}} R_n^{(\mathrm{l})} L_{n-1} - b_{\mathrm{int}} S_n^{(\mathrm{l})} + b_{\mathrm{ext}} (1/2 - \beta) S_n^{(\mathrm{i})},
\end{aligned} \quad \text{(B1)}$$

with the kinetics for the remaining quantities as in Eq. (1). For $\beta = -1/2$, all receptor-bound ligands are externalized on the left surface, for $\beta = 1/2$ on the right surface, and for $\beta = 0$, we recover the unbiased description. This implies that the externalization of the free receptors remains unbiased. We proceed as before to derive the continuum equations. The adiabatic approximation changes to

$$s_- = \frac{k_{\mathrm{on}} a l r_- - 2\beta b_{\mathrm{ext}} s_i - \frac{a b k_{\mathrm{on}}}{2} r_+ \partial_x l + \frac{(a-b) b_{\mathrm{ext}}}{2} \partial_x s_i}{b_{\mathrm{int}} + k_{\mathrm{off}}} \quad \text{(B2)}$$

with the other relations as in Eq. (5). Finally, the transport equations (6) and (7) generalize to Eq. (9) with the new effective drift velocity

$$V_\beta(\lambda,\rho) = 2a^2\beta b_{\text{ext}}b_{\text{int}}f_{\text{ext}}f_{\text{int}}k_{\text{off}}k_{\text{on}}\rho(b_{\text{ext}}[f_{\text{int}}(b_{\text{int}}+k_{\text{off}}) + ab_{\text{int}}k_{\text{on}}\lambda][(f_{\text{ext}}+f_{\text{int}})k_{\text{off}} + af_{\text{ext}}k_{\text{on}}\lambda] + ab_{\text{ext}}f_{\text{ext}}k_{\text{on}}[f_{\text{int}}(b_{\text{int}}+k_{\text{off}}) - ab_{\text{int}}k_{\text{on}}\lambda]\rho + [f_{\text{int}}(b_{\text{int}}+k_{\text{off}}) + ab_{\text{int}}k_{\text{on}}\lambda]A(\lambda,\rho) + ab_{\text{int}}f_{\text{ext}}k_{\text{on}}\{f_{\text{int}}k_{\text{off}}(\lambda+\rho) + b_{\text{int}}[ak_{\text{on}}\lambda(\lambda-\rho) + f_{\text{int}}(\lambda+\rho)]\})^{-1}, \tag{B3}$$

where $A(\lambda,\rho)$ is defined in Eq. (A6). The other coefficients appearing in Eq. (9) remain as in the case without directional bias.

APPENDIX C: SIMPLE LIMITS OF THE EFFECTIVE TRANSPORT EQUATIONS

In biological systems, it is well possible that some of the processes included in our description of ligand transport are much faster than the others. For example, the binding of the ligand to its receptor can be fast compared to other processes due to the small volume of the gaps between cells. The confinement of the ligands to this small volume leads to frequent collisions between ligands and receptors. Assuming that the reaction is diffusion limited this can lead to a high reaction rate k_{on}.

It is worthwhile to note that Eqs. (6) and (7) become simpler if this or another one of the cellular processes is much faster than the others, i.e., if the corresponding rates in our description are very large. For example, in the limit of very fast binding of ligands to receptors, i.e., for $k_{\text{on}}\to\infty$, we find

$$D_\lambda(\lambda,\rho) = \frac{-a^2b_{\text{ext}}b_{\text{int}}f_{\text{ext}}f_{\text{int}}k_{\text{off}}\rho}{B(\lambda,\rho)},$$

$$D_\rho(\lambda,\rho) = \frac{a^2b_{\text{ext}}b_{\text{int}}f_{\text{ext}}f_{\text{int}}k_{\text{off}}\lambda}{B(\lambda,\rho)},$$

$$k_\lambda(\lambda,\rho) = \frac{b_{\text{deg}}b_{\text{int}}}{b_{\text{ext}}+b_{\text{int}}},$$

$$k_\rho(\lambda,\rho) = \frac{b_{\text{deg}}b_{\text{int}}(f_{\text{ext}}+f_{\text{int}})\lambda + (b_{\text{ext}}+b_{\text{int}})f_{\text{deg}}f_{\text{int}}(\rho-\lambda)}{(b_{\text{ext}}+b_{\text{int}})(f_{\text{ext}}+f_{\text{int}})\rho}, \tag{C1}$$

where

$$B(\lambda,\rho) = 4\{b_{\text{int}}f_{\text{ext}}f_{\text{int}}(b_{\text{int}}+k_{\text{off}}) + b_{\text{ext}}[b_{\text{int}}f_{\text{ext}}f_{\text{int}} + f_{\text{ext}}f_{\text{int}}k_{\text{off}} - b_{\text{int}}(f_{\text{ext}}+f_{\text{int}})k_{\text{off}}]\}\lambda - 4(b_{\text{ext}}+b_{\text{int}})f_{\text{ext}}f_{\text{int}}(b_{\text{int}}+k_{\text{off}})\rho.$$

There are no free ligands in this limit because $l=0$ via Eq. (5). As all ligands are bound to receptors, free diffusion does not contribute to the current and D_0 does not appear in Eq. (C1). This also imposes the constraint $\lambda\leqslant\rho$. The example given by Eq. (C1) is instructive because the effective transport and degradation coefficients are much simpler than those in the general case (A6). Many of the properties discussed above for the general case that is valid for arbitrary k_{on} can be read directly from the expressions in Eq. (C1). For example, if $b_{\text{ext}}=0$ ligands do not move because $D_\lambda=D_\rho=0$ in Eq. (C1). Due to the constraint $\lambda\leqslant\rho$, however, the statements for the asymptotic behavior for $\lambda\to\infty$ do not apply to this case. Furthermore, D_λ does no longer exhibit a maximum as a function of λ. It either grows or decreases monotonically depending on the parameter choice.

In principle, one can write down simpler expressions as in Eq. (C1) for many different limits. If several transport steps are much faster than the others, only the ratios of the corresponding parameters enter the simplified description. For example, if the binding and unbinding of the ligand to the receptor is faster than all other processes the effective diffusion coefficient and degradation rate do not depend on k_{on} and k_{off} individually but only on the ratio $k_{\text{on}}/k_{\text{off}}$. The number of parameters can thus be reduced to obtain the minimal description for a given situation. A simple but instructive example is the situation $k_{\text{on}}\gg k_{\text{off}}\gg b_{\text{ext}}\gg b_{\text{int}}$ in Eq. (11), for which we obtain the effective diffusion coefficient

$$\lim_{b_{\text{ext}}\to\infty}\lim_{k_{\text{off}}\to\infty}\lim_{k_{\text{on}}\to\infty} D(\lambda) = b_{\text{int}}a^2/4.$$

This reflects that the only slow process—in this case the internalization of ligands at rate b_{int}—limits the transport efficiency and defines the effective diffusion coefficient. Note, that the limits taken above do not commute because $D(\lambda)=0$ for $k_{\text{off}}\gg k_{\text{on}}$.

APPENDIX D: TRANSPORT BY DIFFUSION IN THE CELL MEMBRANE

As another example for an application of our theoretical framework, consider a transport mechanism in which ligands can move across cells by passive diffusion in the cell membrane. The ligand first binds to a receptor molecule on the cell surface. This complex then diffuses in the cell membrane. At any time, the ligand can detach from the receptor it occupies and, after diffusing over a short distance in the extracellular space, it can attach to a new receptor that can be located on the surface of the same or a different cell. Note, that if we simply replace the receptors with HSPG molecules this transport mechanism is very similar to one that was recently suggested for Dpp in the wing disk [11].

We can describe this mechanism on the same lattice structure as used above for transcytosis, see Fig. 1. For simplicity, we focus on the essence of the transport phenomenon and do not include ligand degradation or the production and degradation of receptors in our description. Furthermore, the receptor concentration is assumed to be constant on the cell surface. This description is similar to that of transcytosis with constant surface receptor concentration given by Eq. (10). However, instead of the internalization and externalization of receptor-ligand complexes as in transcytosis, dislocation of the ligand-receptor complexes across one cell is due to diffusion on the cell surface. In a discrete one-dimensional description, this effect is captured by hopping at a rate $h\simeq D_M/2a^2$ between the left and right surface of each cell,

where D_M is the diffusion coefficient of receptors in the cell membrane. Using the same notation as in Eq. (10), a discrete description of this mechanism reads

$$\frac{d}{dt}L_n = k_{\text{off}}(S_n^{(\text{r})} + S_{n+1}^{(\text{l})}) - k_{\text{on}}(R - S_n^{(\text{r})} - S_{n+1}^{(\text{l})})L_n,$$

$$\frac{d}{dt}S_n^{(\text{r})} = -k_{\text{off}}S_n^{(\text{r})} + k_{\text{on}}(R/2 - S_n^{(\text{r})})L_n + h(S_n^{(\text{l})} - S_n^{(\text{r})}),$$

$$\frac{d}{dt}S_n^{(\text{l})} = -k_{\text{off}}S_n^{(\text{l})} + k_{\text{on}}(R/2 - S_n^{(\text{l})})L_{n-1} + h(S_n^{(\text{r})} - S_n^{(\text{l})}).$$

Applying the same method as in Sec. III B, we obtain the continuum transport equation $\partial_t\lambda = \partial_x(D_{\text{SD}}(\lambda)\partial_x\lambda)$ where λ is the total ligand concentration and

$$D_{\text{SD}}(\lambda) = \frac{a^3 rhk_{\text{off}}k_{\text{on}}[E(\lambda) - k_{\text{off}} + ak_{\text{on}}(-\lambda + r)]}{4E(\lambda)[E(\lambda)h - h(k_{\text{off}} + ak_{\text{on}}\lambda) + ar(h + k_{\text{off}})k_{\text{on}}]},$$

with

$$E(\lambda) = \{-4a^2 rk_{\text{on}}{}^2\lambda + [k_{\text{off}} + ak_{\text{on}}(r + \lambda)]^2\}^{1/2}. \quad \text{(D1)}$$

$D_{\text{SD}}(\lambda)$ has properties that are similar to those of the effective diffusion coefficient of the transcytosis model. It exhibits a maximum as a function of λ and decays as $D_{\text{SD}} \sim \lambda^{-2}$ for large λ. Hence, upon inclusion of ligand degradation in the description, gradient formation by this mechanism exhibits similar properties as transcytosis.

APPENDIX E: TRANSPORT BY EXTRACELLULAR DIFFUSION

In order to ultimately identify the mechanism of morphogen gradient formation present in a given system, it is important to develop mathematical descriptions of all potentially relevant transport mechanisms so that these can be compared to the available experimental data. Extracellular diffusion is widely believed to be the dominant transport mechanism for some morphogens [8,14]. For this reason, we briefly discuss the extracellular diffusion dominated limit of the transport phenomenon defined by Eq. (1) in this section.

Assuming that extracellular diffusion gives the dominant contribution to the ligand current, we neglect the contribution of transcytosis. This approach is valid if the rates of ligand trafficking are such that the effective diffusion coefficient resulting from transcytosis $D(\lambda,\rho)|_{p=0}$ in Eq. (6) is much smaller for all values of λ and ρ than the extracellular diffusion constant D_0.

The derivation of the continuum limit of Eq. (1) is straightforward in this situation. Only the equation for the time development of the free ligand concentration contains a linear diffusion term. All other quantities can be described by a coupled set of ordinary differential equations. Together, these constitute a set of reaction-diffusion equations. With the notation used throughout this article, the kinetic equations in two dimensions read

$$\partial_t l = D_0\Delta l - k_{\text{on}}a^2 l r_+ + k_{\text{off}}s_+ - e_{\text{deg}}l,$$

$$\partial_t s_+ = k_{\text{on}}a^2 l r_+ - (b_{\text{int}} + k_{\text{off}})s_+ + b_{\text{ext}}s_i,$$

$$\partial_t s_i = b_{\text{int}}s_+ - (b_{\text{ext}} + b_{\text{deg}})s_i,$$

$$\partial_t r_+ = \frac{f_{\text{syn}}}{a^2} + k_{\text{off}}s_+ + f_{\text{ext}}r_i - k_{\text{on}}l r_+ - f_{\text{int}}r_+,$$

$$\partial_t r_i = f_{\text{int}}r_+ - (f_{\text{ext}} + f_{\text{deg}})r_i. \quad \text{(E1)}$$

This is essentially the system that was previously studied in [13,14]. This reaction-diffusion system can reproduce some experimental results that were obtained for the morphogen Dpp and its receptor Tkv in the wing disk [13,14]. However, there are experimental observations that are in disagreement with the solutions of Eq. (E1) indicating that this is not a correct description of the ligand and receptor kinetics in this system [6,13]. In other experimental systems, reaction-diffusion mechanisms may play a role in pattern formation during development [2,28,29].

[1] T. Tabata and Y. Takei, Development **131**, 703 (2004).
[2] A. M. Turing, Philos. Trans. R. Soc. London, Ser. B **237**, 37 (1952).
[3] L. Wolpert, J. Theor. Biol. **25**, 1 (1969).
[4] W. Driever and C. Nüsslein-Volhard, Cell **54**, 83 (1988).
[5] W. Driever and C. Nüsslein-Volhard, Cell **54**, 95 (1988).
[6] E. V. Entchev, A. Schwabedissen, and M. González-Gaitán, Cell **103**, 981 (2000).
[7] A. A. Teleman and S. M. Cohen, Cell **103**, 971 (2000).
[8] J. B. Gurdon, P. Harger, A. Mitchell, and P. Lemaire, Nature (London) **371**, 487 (1994).
[9] F. Crick, Nature (London) **225**, 420 (1970).
[10] N. McDowell, A. M. Zorn, D. J. Crease, and J. B. Gurdon, Curr. Biol. **7**, 671 (1997).
[11] T. Y. Belenkaya, C. Han, D. Yan, R. J. Opoka, M. Khodoun, and X. Lin, Cell **119**, 231 (2004).
[12] F. A. Ramirez-Weber and T. B. Kornberg, Cell **97**, 599 (1999).
[13] K. Kruse, P. Pantazis, T. Bollenbach, F. Jülicher, and M. González-Gaitán, Development **131**, 4843 (2004).
[14] A. D. Lander, Q. Nie, and F. Y. M. Wan, Dev. Cell **2**, 785 (2002).
[15] B. Houchmandzadeh, E. Wieschaus, and S. Leibler, Nature (London) **415**, 798 (2002).
[16] T. Gregor, W. Bialek, R. R. de Ruyter van Stevenick, D. W. Tank, and E. F. Wieschaus, Proc. Natl. Acad. Sci. U.S.A. **102**, 18403 (2005).
[17] S. Morimura, L. Maves, Y. Chen, and F. Hoffmann, Dev. Biol. (Orlando, FL, U.S.) **177**, 136 (1996).
[18] A. Eldar, R. Dorfman, D. Weiss, H. Ashe, B. Z. Shilo, and N. Barkai, Nature (London) **419**, 304 (2002).

[19] A. Eldar, D. Rosin, B. Z. Shilo, and N. Barkai, Dev. Cell **5**, 635 (2003).
[20] T. Bollenbach, K. Kruse, P. Pantazis, M. González-Gaitán, and F. Jülicher, Phys. Rev. Lett. **94**, 018103 (2005).
[21] M. Howard and P. R. ten Wolde, Phys. Rev. Lett. **95**, 208103 (2005).
[22] G. Hornung, B. Berkowitz, and N. Barkai, Phys. Rev. E **72**, 041916 (2005).
[23] M. Kerszberg and L. Wolpert, J. Theor. Biol. **191**, 103 (1998).
[24] Y. Chen and G. Struhl, Cell **87**, 553 (1996).
[25] D. A. Lauffenburger and J. J. Lindermann, *Receptors: Models for Binding, Trafficking, and Signaling* (Oxford University Press, Oxford, UK, 1993).
[26] C. Han, T. Y. Belenkaya, B. Wang, and X. H. Lin, Development **131**, 601 (2004).
[27] B. Shraiman, Proc. Natl. Acad. Sci. U.S.A. **102**, 3318 (2005).
[28] H. Meinhardt, *Models of Biological Pattern Formation* (Academic, London, 1982).
[29] A. J. Koch and H. Meinhardt, Rev. Mod. Phys. **66**, 1481 (1994).